THE PENNSYLVANIA STATE UNIVERSITY
SCHREYER HONORS COLLEGE

DEPARTMENT OF ELECTRICAL ENGINEERING

CONVERSION GAIN AND SENSITIVITY IN MARGINAL OSCILLATORS: CONTINUOUS AND SAMPLED-DATA NEGATIVE RESISTANCE CONVERTERS

KLAUS K. ZHANG
Spring 2011

A thesis
submitted in partial fulfillment
of the requirements
for a baccalaureate degree
in Electrical Engineering
with honors in Electrical Engineering

Reviewed and approved* by the following:

Jeffrey L. Schiano
Associate Professor of Electrical Engineering
Thesis Supervisor

John D. Mitchell
Professor of Electrical Engineering
Honors Adviser

*Signatures are on file in the Schreyer Honors College.

Abstract

A marginal oscillator is an instrument used to detect changes in the losses of a tuned circuit. It consists of a parallel RLC circuit driven by a dependent current source that is controlled by the voltage across the RLC circuit. The dependent current source implements a nonlinear negative resistance converter that injects just enough energy to overcome the resistive losses and thereby produce a steady-state oscillation in the voltage across the circuit. The main figure of merit for a marginal oscillator is its conversion gain, which relates the change in the amplitude of oscillation to the change in the losses of the tuned circuit. Viswanathan showed that the conversion gain depends on the shape of the nonlinear negative resistance converter. In general, a higher conversion gain is desired. An earlier study that simulated the marginal oscillator yielded estimates of the conversion gain that were not consistent with theoretical predictions. The objectives of this thesis are threefold. First, we want to reconcile the difference between theory and simulation by choosing an appropriate integration algorithm and its parameters. This thesis shows that by appropriately choosing the integration algorithm and its parameters, the simulation results are in agreement with the theoretical predictions. The second objective is to investigate the feasibility of implementing the dependent current source using a data-sampled system in place of analog circuitry in order to facilitate the implementation of nonlinear characteristics that maximize conversion gain. Specifically, this study uses numerical simulation to determine the effects of quantization in time and amplitude on the the conversion gain. The third objective is to numerically determine the sensitivity of the marginal oscillator, which is the smallest change in losses that can be detected in the presence of thermal noise for a given conversion gain.

Table of Contents

List of Figures

List of Tables

Acknowledgments

This thesis could not have been written without Dr. Jeff Schiano, who guided me through this research project. He encouraged and challenged me, and he never accepted less than my best efforts. Thank you.

I would like to thank Penn State, The Schreyer Honors College, and all of my professors for their involvement in my education.

Most especially, I would like to thank my family, friends, and my luminous and loving girlfriend, Elyssa Okkelberg. I am grateful for their support and motivation.

Chapter 1

Marginal Oscillators

1.1 Applications

A marginal oscillator is an instrument for detecting losses in the electrical properties of a tuned circuit. Roberts and Rollins credit Pound with developing the marginal oscillator in the 1940s for use in nuclear resonance spectroscopy experiments [1, 2]. Pound demonstrated that a marginal oscillator can detect the absorption of radio frequency energy by the nuclei of a solid material [3]. By measuring the change in absorption as a function of frequency, Pound was able to investigate the molecular structure of the solid.

Recent applications of marginal oscillators include characterization of defects in silicon [4], measurement of the penetration depth of superconductors [5], ion cyclotron resonance spectroscopy [6, 7], and investigation of the mechanical properties of thin-films [8]. Additionally, they can be used for monitoring the curing of plastics [9] and precision measurement of both capacitances [10] and very low temperatures [11].

1.2 Conceptual Model

Figure 1.1 represents a marginal oscillator as a parallel resonant circuit driven by a voltage-controlled current source. A parallel RLC network represents the resonant circuit. The inductance L and capacitance C of the network determine the frequency of oscillation, and the losses within the network are represented by the resistance R. To maintain a steady-state sinusoidal oscillation, the dependent current source must supply just enough energy to counter these losses. In other words, the dependent current source must appear as a negative resistance with value $-R$, so that the parallel LC network sees an open circuit. Therefore, the dependent current source represents a negative resistance converter (NRC). The overall circuit is called a marginal oscillator because the dependent source provides just enough energy to sustain oscillation.

As will be shown in Chapter 2, it is desirable to implement the dependent current source so

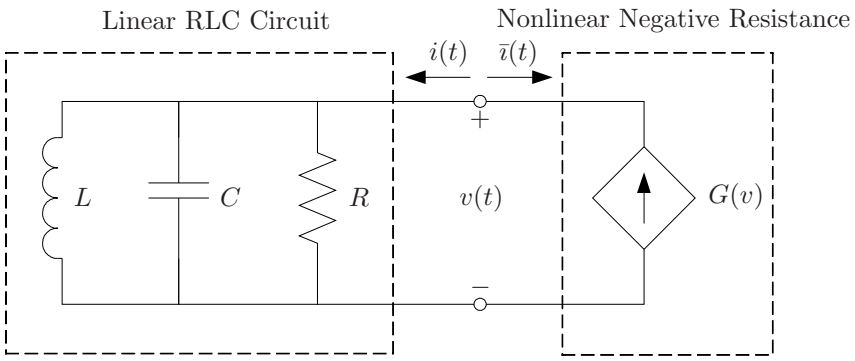

Figure 1.1. Schematic representation of a marginal oscillator.

that the current is a nonlinear function of the input voltage $v(t)$. In short, the gain between the output current and the input voltage is dependent on the amplitude of $v(t)$. Pound was the first to implement a marginal oscillator. His implementation used the nonlinear characteristic of a vacuum tube to produce $G(v)$ [3]. As the input voltage to the vacuum tube increases, its gain, and hence the feedback current $i(t)$ to the RLC circuit, decreases.

1.3 Figures of Merit

The main figure of merit of a marginal oscillator is the sensitivity of the amplitude of oscillation with respect to the losses in the resonance circuit. This sensitivity is defined as

$$S_R^A = \frac{\%\text{ change in A}}{\%\text{ change in R}} = \frac{\Delta A/A}{\Delta R/R}, \tag{1.1}$$

where A and R represent the nominal amplitude and losses, while ΔA represents the change in amplitude due to a change ΔR in losses. In the limit as ΔR approaches zero,

$$S_R^A = \frac{\partial A}{\partial R}\frac{R}{A}. \tag{1.2}$$

This definition is consistent with signal processing and control systems usage. However, physicists often use the term sensitivity to indicate the smallest change in root mean square (rms) voltage that can be seen above the noise floor in a circuit. In order to avoid confusion between the two terms, this paper uses the convention of Viswanathan [12] and refers to the sensitivity defined in Eq. (1.1) as the conversion gain

$$G_c = S_R^A. \tag{1.3}$$

In general, we want the conversion gain to be as large as possible.

To understand why a large conversion gain is useful, consider the conversion gain of a Q-meter, where the dependent current source in Figure 1.1 is replaced by a independent sinusoidal

current source whose frequency is $1/\sqrt{LC}$. Suppose that the current source is chosen so that

$$i(t) = I_0 \cos\left(\frac{1}{\sqrt{LC}}t\right), \tag{1.4}$$

independent of $v(t)$. Using phasor analysis, the sinusoidal steady-state voltage across the resonant circuit is

$$v(t) = RI_0 \cos\left(\frac{1}{\sqrt{LC}}t\right) = A\cos\left(\frac{1}{\sqrt{LC}}t\right), \tag{1.5}$$

where A is the oscillation amplitude. It follows that the conversion gain of a Q-meter is

$$G_c = \frac{R}{A}\frac{\partial A}{\partial R} = \frac{R}{RI_0}\frac{\partial RI_0}{\partial R} = 1. \tag{1.6}$$

In a typical magnetic resonance experiment, the normalized change in R, $\Delta R/R$, is on the order of 10^{-6}. As the nominal amplitude A of oscillation is about 1 V and the conversion gain is unity, the change in A is about 1 μV. In order to improve the signal-to-noise ratio (SNR) when measuring a change in amplitude ΔA, a higher conversion gain is needed.

In 1950, Pound was the first to recognize that significantly larger conversion gains could be achieved by replacing the independent current source in the Q-meter with a dependent current source. The resulting feedback path not only generates a sinusoidal signal but also increases the conversion gain. However, Pound did not analyze how the form of the feedback $G(v)$ affects the conversion gain. It was not until the mid-1970s that Viswanathan analytically computed the conversion gain and showed it is determined by the shape of $G(v)$. Conversion gains on the order of 10 to 100 have been achieved in experiments.

Another figure of merit of the marginal oscillator is the sensitivity, that Adler defined as the minimum change in oscillation amplitude that can be detected in the presence of thermal noise due to losses in the resonant circuit [13]. This method does not directly take into consideration the conversion gain and how it affects the sensitivity. For this reason, this thesis introduces another definition of the sensitivity of a marginal oscillator. The new definition is motivated by the concept of noise factor (NF) and the noise figure, $10\log_{10}(\text{NF})$, which are figures of merit for amplifiers. The NF specifies the amount of noise introduced by a device. For an amplifier, the NF is the ratio of the SNR of the input to the SNR of the output. Ideally, the NF of an amplifier is unity, but in practice, because amplifiers always add noise, the NF is always greater than unity. This study defines the NF for a marginal oscillator in a similar manner by comparing the SNR of a marginal oscillator to the SNR of a Q-meter. The reason for doing this is the SNR for a marginal oscillator is dependent on its conversion gain so we want to compare that SNR to the SNR of a Q-meter whose conversion gain is unity. For both a marginal oscillator and a Q-meter, define the SNR as the ratio of the rms envelope voltage due to changes in the losses of the resonant circuit to the rms envelope voltage due to thermal noise. Using this definition of SNR, the NF for a marginal oscillator is defined as the ratio of the SNR of a Q-meter to the SNR of the marginal oscillator. Unlike the case for an amplifier, the restriction that NF is greater

than unity may not hold due to the nonlinearities of the marginal oscillator.

1.4 Thesis Contributions

The specific aims of this thesis are threefold. The first aim is to compare the simulated amplitude, frequency, and conversion gain with theoretical predictions. This goal requires selection of an appropriate solver and solver parameters, along with defining a protocol for estimating conversion gain from simulation results. The second aim is to use simulation results to determine the viability of implementing a marginal oscillator where the NRC is realized using a digital signal processing (DSP) system. In particular, the aim is to determine how the sample rate and quantization of the output levels affect the conversion gain of a marginal oscillator that uses a sampled-data NRC. The third aim is to numerically determine the sensitivity of the marginal oscillator by including a noise source that models the thermal noise due to the losses of the resonant circuit.

Miller made an early attempt to compare the conversion gains from theory, simulation, and experiment [14], but he was unsuccessful for two reasons. First, the simulation used a poor choice of integration algorithm. A nonstiff solver was used while a marginal oscillator is a stiff system. Second, Miller did not take into account that the amplitude A is a nonlinear function of the losses R when calculating the conversion gain using Eq. (1.1). The ratio $\Delta A/\Delta R$ used in that equation needs a small ΔR in order to accurately approximate the partial derivative in Eq. (1.2).

This thesis shows that Viswanathan's theoretical prediction closely matches Matlab simulation results. This result was achieved in two steps. First, by reviewing properties of integration algorithms and methods for doing simulation, this thesis shows how to accurately simulate the behavior of the model. Second, taking into account the strong nonlinear relationship of A and R, a protocol for calculating conversion gain is realized. Using the protocol, the simulation matches Viswanathan's prediction. Furthermore, this study revealed that it is possible to simulate the marginal oscillator in Simulink rather than an m-file exclusively, resulting a decrease in simulation time by a factor of 100 due to the reduced number of function calls needed when using Simulink.

The second aim of the thesis is to show the feasibility of implementing the NRC using a sampled-data system. This is desirable as it facilitates NRC functions tailored to increase the conversion gain. As a first step, this thesis shows it is possible to replace the continuous-time feedback $i(t) = G(v)$ with a sampled-time implementation $i(k) = G(v(k))$, where time is quantized but amplitude is not. The second step is to investigate what happens when the amplitude is also quantized, for a sampled-data implementation. In short, larger gains are needed in the feedback path when the NRC is implemented using a sampled-data system. This result was found by simulation, not theory. Finally, this thesis investigates how to implement the NRC using a discrete-time DSP system.

The third aim is to take into account the effect of thermal noise on the marginal oscillator by including a white noise generator in the simulation model. The noise source accounts for the thermal noise of the losses in the resonant circuit, and for simplicity, ignores the contribution

of noise by the NRC. This facilitates numerical calculation of the noise factor of the marginal oscillator, as previously defined. In addition, incorporation of thermal noise enables a study of the trade-offs among measurement bandwidth, conversion gain, and noise factor.

The remainder of the thesis is organized as follows. Chapter 2 describes the design of a marginal oscillator and the figures of merit. Chapter 3 describes the implementation of the simulation model and discusses the simulation results. Chapter 4 provides a summary and discussion of the work.

Chapter 2

Design and Figures of Merit

For the purpose of analysis, it is convenient to represent the marginal oscillator as the feedback network in Figure 2.1. This form separates the marginal oscillator into a linear time-invariant resonant circuit represented by the transfer function $H(s) = V(s)/I(s)$ and a feedback block represented by the memoryless nonlinearity $G(v)$.

Section 2.1 motivates the designs of the resonant circuit and the NRC by investigating a model of the marginal oscillator as a nonlinear, second-order ordinary differential equation (ODE). Section 2.2 shows how to represent the linear RLC circuit using a transfer function and state-space representation. Section 2.3 shows that the nonlinear feedback element realizes a NRC and discusses techniques for realizing a NRC. A discussion of the conversion gain is given in Section 2.4. Section 2.5 defines the sensitivity and noise figure of a marginal oscillator.

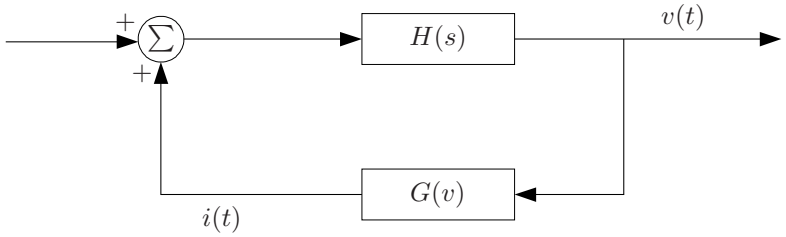

Figure 2.1. Feedback system representation of marginal oscillator.

2.1 Marginal Oscillator

The RLC circuit in Figure 1.1, with an input current $i(t)$ and a voltage $v(t)$ across it, can be represented by the ODE

$$\frac{d^2v}{dt^2} + \frac{1}{RC}\frac{dv}{dt} + \frac{1}{LC}v = \frac{1}{C}\frac{di}{dt}. \tag{2.1}$$

Substituting $i(t) = G(v)$, which represents the NRC, and defining

$$g(v) = \frac{dG(v)}{dv} \tag{2.2}$$

leads to the following representation of the marginal oscillator,

$$\frac{d^2v}{dt^2} + \frac{1}{C}\left(\frac{1}{R} - g(v)\right)\frac{dv}{dt} + \frac{1}{LC}v = 0. \tag{2.3}$$

Note that the conductance looking into the dependent current source, at a particular voltage v, is

$$-\frac{di}{dv} = -\frac{dG(v)}{dv} = -g(v). \tag{2.4}$$

If the dependent source is implemented as $G(v) = v/R$, then the conductance looking into it is $-1/R$ and the representation of the marginal oscillator in Eq. (2.3) reduces to the undamped second-order ODE

$$\frac{d^2v}{dt^2} + \frac{1}{LC}v = 0 \tag{2.5}$$

that admits a steady-state sinusoidal oscillation with a frequency of $1/\sqrt{LC}$.

In practice, it is difficult to have $g(v)$ match $1/R$ exactly. When $g(v)$ is less than $1/R$, the amplitude of oscillation decays exponentially, and when $g(v)$ is greater than $1/R$, the amplitude of oscillation tends to infinity. Instead, one uses a nonlinear function $G(v)$ that represents a conductance that varies with the voltage $v(t)$. In this case, the marginal oscillator achieves a steady-state oscillation whose amplitude is determined by both the losses R in the RLC circuit and the shape of the nonlinear function $G(v)$ [12].

2.2 Resonant Circuit

The transfer function of the resonant circuit follows directly by taking the Laplace transform of Eq. (2.1),

$$H(s) = \frac{V(s)}{I(s)} = \frac{\frac{1}{C}s}{s^2 + \frac{1}{RC}s + \frac{1}{LC}}, \tag{2.6}$$

and represents the impedance looking into the RLC circuit. The transfer function $H(s)$ has a Bode magnitude plot with a bandpass filter shape. The peak magnitude occurs at the natural frequency $\omega_n = 1/\sqrt{LC}$ and is $H(j\omega_n) = R$. The 3 dB bandwidth is $\beta = 1/RC$. It is useful to characterize the transfer function by the quality factor, or Q-factor, which is defined as

$$Q = 2\pi \times \frac{\text{Energy stored}}{\text{Energy dissipated per cycle}}. \tag{2.7}$$

Using the above definition, it is straight forward to show that $Q = R/\omega_n L$ for the resonant circuit. In signal processing, the Q-factor is defined as the peak frequency divided by the 3 dB

bandwidth. For the resonant circuit at the peak frequency, the two definitions are identical, and

$$Q = \frac{R}{\omega_n L} = \frac{\omega_n}{\beta}. \tag{2.8}$$

In general, a high Q-factor is desirable because it indicates a narrow bandwidth, decreasing the effect of thermal noise. It is useful to write the transfer function as

$$H(s) = \frac{\frac{1}{C}s}{s^2 + \frac{\omega_n}{Q}s + \omega_n^2}, \tag{2.9}$$

in terms of the Q-factor and the natural frequency ω_n.

For ease of numerical simulation, it is useful to represent the resonant circuit by an all-integrator block diagram. The all-integrator block diagram is derived from a state-space representation using the physical variable definition, where the state variables are chosen to represent the stored energy in the resonant circuit. In particular, scaled versions of the inductor current and the capacitor voltage are used, where the scaling is chosen so that the system matrix can written in terms of the natural frequency ω_n and the Q-factor. Choosing $x_1 = LCi_L(t)$, where $i_L(t)$ is the inductor current, and $x_2 = Cv(t)$ achieves this goal and results in the state-space representation

$$\begin{pmatrix} \dot{x_1} \\ \dot{x_2} \end{pmatrix} = \begin{pmatrix} 0 & 1 \\ -\omega_n^2 & -\frac{\omega_n}{Q} \end{pmatrix} \begin{pmatrix} x_1 \\ x_2 \end{pmatrix} + \begin{pmatrix} 0 \\ 1 \end{pmatrix} i(t) \tag{2.10}$$

$$v(t) = \begin{pmatrix} 0 & \frac{1}{C} \end{pmatrix} \begin{pmatrix} x_1 \\ x_2 \end{pmatrix}. \tag{2.11}$$

Using the state-space representation in Eqs. (2.10) and (2.11), the corresponding all-integrator block diagram is shown in Figure 2.2. In terms of the inductor current and capacitor voltage, the initial conditions are

$$x_1(0) = LCi_L(0) \tag{2.12}$$

$$x_2(0) = Cv(0). \tag{2.13}$$

2.3 Negative Resistance Converter

This thesis considers a NRC realized by a dependent current source $i = G(v)$ in Figure 2.3a, whose current-voltage (i-v) characteristics are shown in Figure 2.3b. This particular form is useful for two reasons. First, it is a good representation of the i-v characteristics of marginal oscillator feedback circuits made using vacuum tubes and FETs. Second, this piecewise-linear form facilitates analytical calculation of conversion gain. As shown in Figure 2.3b, when the

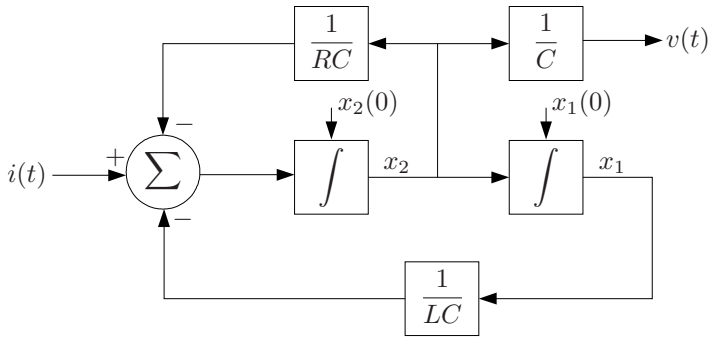

Figure 2.2. All-integrator block diagram of resonant circuit.

magnitude of the input voltage is less than some threshold v_T, the dependent source appears as a gain block with gain g_A. However, when the magnitude exceeds v_T, the gain rolls off to g_B.

To understand why the dependent current source realizes a NRC, use the definition of $\bar{\imath}$ in Figure 2.3a,

$$\bar{\imath} = -G(v). \tag{2.14}$$

The conductance looking into the dependent current source at a given input voltage v^* is

$$\text{conductance}|_{v^*} = \left.\frac{\Delta\bar{\imath}}{\Delta v}\right|_{v^*} = \left.\frac{d\bar{\imath}}{dv}\right|_{v^*} = -\left.\frac{dG(v)}{dv}\right|_{v^*} = -g(v^*). \tag{2.15}$$

For $G(v)$ of the form shown in Figure 2.3b, the slope $g(v)$ is shown in Figure 2.4. By the definition in Eq. (2.15), the conductance is negative for all voltages. Therefore, the resistance is also negative, and the dependent current source is a NRC.

In order to implement the NRC using either an analog circuit or a sampled-data system using a dedicated signal processing chip, it is useful to represent the NRC using the dependent voltage source $\overline{G}(v)$ in series with the feedback resistance R_f in Figure 2.5a, rather than a dependent

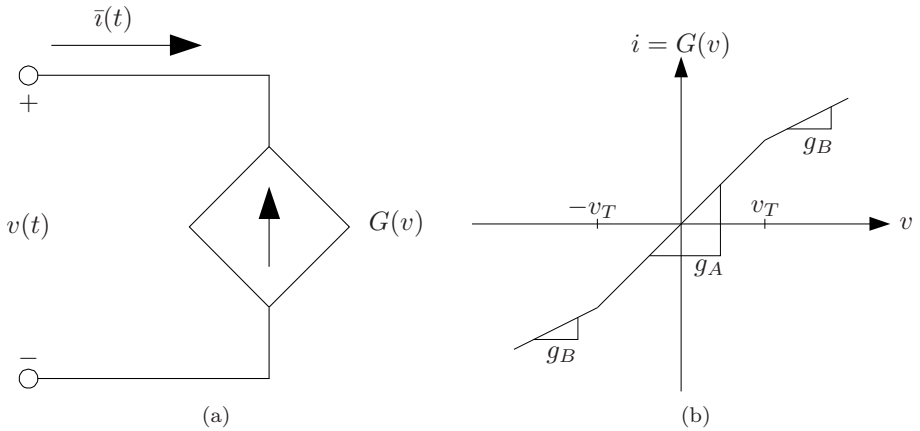

Figure 2.3. (a) Dependent current source (b) Current-voltage (i-v) characteristic.

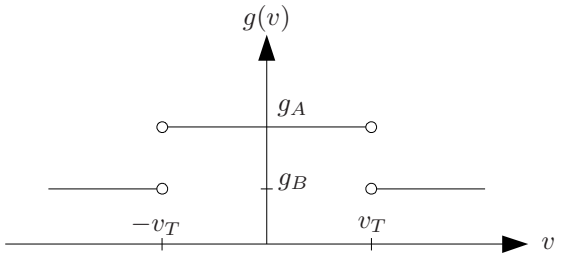

Figure 2.4. Voltage-dependent conductance.

current source. For the circuit in Figure 2.5a,

$$\bar{\imath} = \frac{v - \overline{G}(v)}{R_f}. \tag{2.16}$$

The function $\overline{G}(v)$ is chosen so that the networks in Figures 2.3a and 2.5a have identical i-v characteristics. Using Eq. (2.14) to eliminate $\bar{\imath}$ in Eq. (2.16) leads to

$$\overline{G}(v) = G(v)R_f + v. \tag{2.17}$$

Defining the slope of $\overline{G}(v)$ as

$$\overline{g}(v) = \frac{d\overline{G}(v)}{dv}, \tag{2.18}$$

it follows that

$$\overline{g}(v) = g(v)R_f + 1. \tag{2.19}$$

Given the above expression for $\overline{g}(v)$ and the plot of $g(v)$ in Figure 2.4, it follows that $\overline{G}(v)$ must have the shape shown in Figure 2.5b.

Using the NRC in Figure 2.5a that is realized with a voltage-controlled voltage source, Section

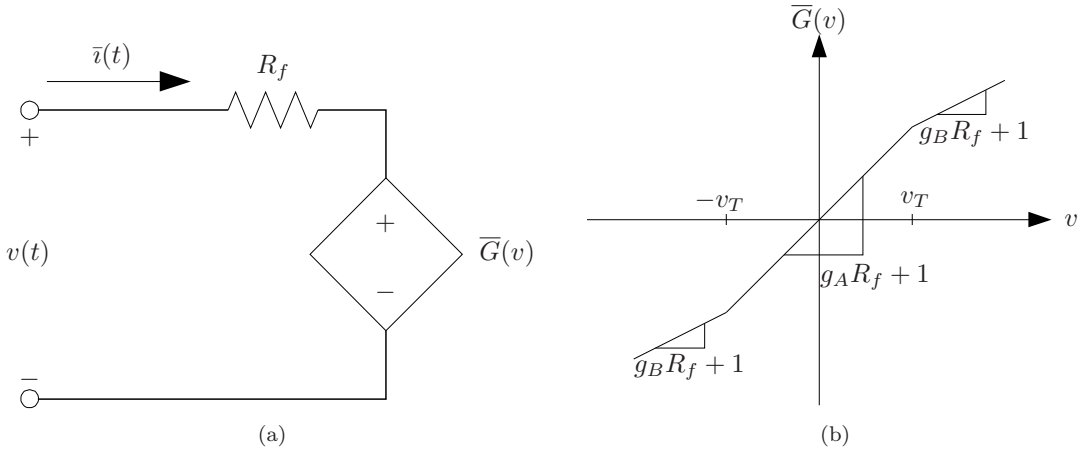

Figure 2.5. (a) NRC with a dependent voltage source (b) Current-voltage (i-v) characteristic of dependent voltage source.

2.3.1 shows how to develop a continuous-time implementation of the NRC using an analog circuit. Then, Section 2.3.2 shows how to extend that result to obtain a sampled-data implementation using a lookup table (LUT) and analog-to-digital and digital-to-analog converters (ADC and DAC).

2.3.1 Analog Implementation

In order to obtain an analog circuit implementation using operational amplifiers, first consider the case where $g_A = g_B$, that is the desired relationship between voltage v and current $\bar{\imath}$ is linear and given by

$$\bar{\imath} = -g_A v. \tag{2.20}$$

Consider the implementation in Figure 2.6a. By comparison with Figure 2.5a, we can see that $\overline{G}(v)$ is implemented by the non-inverting amplifier with a gain of $\alpha+1$. It follows from Eq. (2.16) that

$$\bar{\imath} = \frac{v - \overline{G}(v)}{R_f} = \frac{v - (1-\alpha)v}{R_f} = -\frac{\alpha}{R_f} v. \tag{2.21}$$

Comparing this result to Eq. (2.20),

$$g_A = \frac{\alpha}{R_f}. \tag{2.22}$$

Observe that a desired value of g_A can be obtained by varying the gain of the operational amplifier using α or by varying the feedback resistance R_f.

Now consider the case where the desired i-v characteristic is given by the piecewise-linear curve in Figure 2.3b. The slope needs to decrease from g_A to g_B for $|v| > v_T$. To accomplish this, a voltage divider is used to decrease the value of α. This implementation is shown in

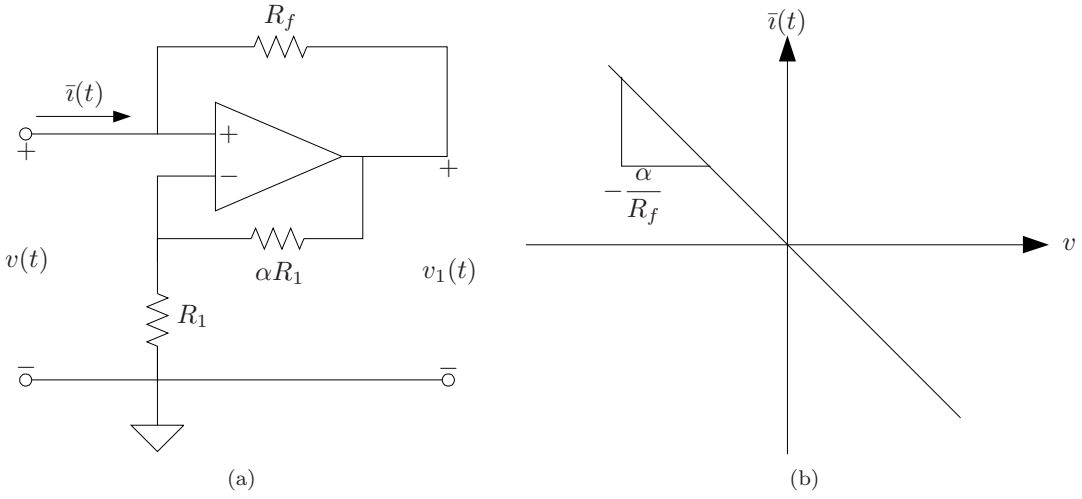

Figure 2.6. (a) Linear analog NRC circuit (b) Current-voltage (i-v) characteristic.

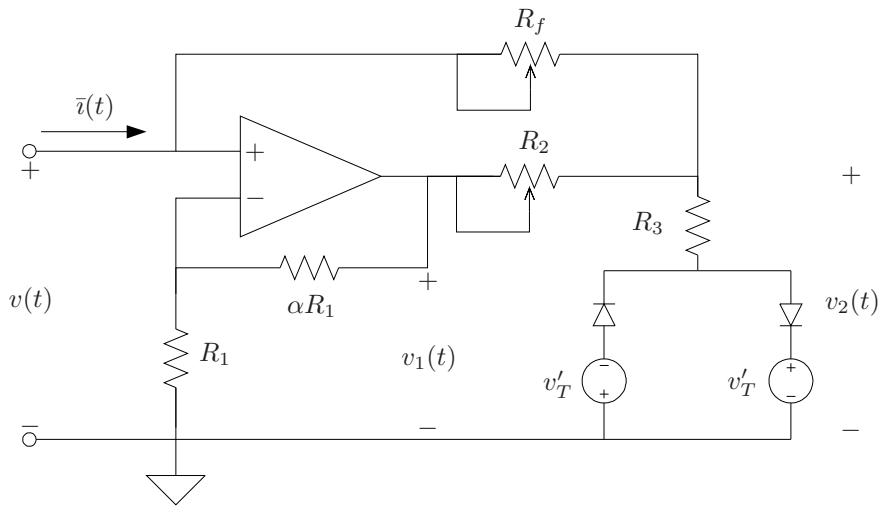

Figure 2.7. An NRC whose i-v characteristics are shown in Figure 2.5b.

Figure 2.7. For $|v| < v_T$, Tricou determined the conductance looking into this circuit is [15]

$$-g_A = -\frac{\alpha}{R_f + R_2}. \tag{2.23}$$

The conductance for $|v| > v_T$ is

$$-g_B = -\frac{\alpha - \dfrac{R_2}{R_5}}{R_f + R_2 + \dfrac{R_f R_2}{R_3}}. \tag{2.24}$$

Suppose that $R_f >> R_2$, $\alpha << 1$, and $R_3 >> R_2$, then the above conductances reduce to

$$-g_A = -\frac{\alpha}{R_f} \tag{2.25}$$

$$-g_B = -\frac{\alpha}{R_f}\left(1 - \frac{R_2}{\alpha R_3}\right). \tag{2.26}$$

This representation shows that g_A can be varied by adjusting either α or R_f as before. Furthermore, the value of g_B can be adjusted by varying R_2. In the circuit implementation, potentiometers are used to realize R_f and R_2, which adjust g_A and g_B, respectively. Figure 2.8 shows a plot of the i-v characteristics of the NRC shown in Figure 2.7. Tricou also shows how to choose the control voltage v'_T to achieve a desired v_T.

This analysis shows that even a simple i-v characteristic described by the three parameters g_A, g_B, and v_T leads to a complicated analog circuit. Studies currently underway to find feedback functions $i = G(v)$ that improve conversion gain will likely lead to even more complicated designs. To simplify the hardware representation of the feedback $i = G(v)$, it would be useful to implement the NRC using a sampled-data system.

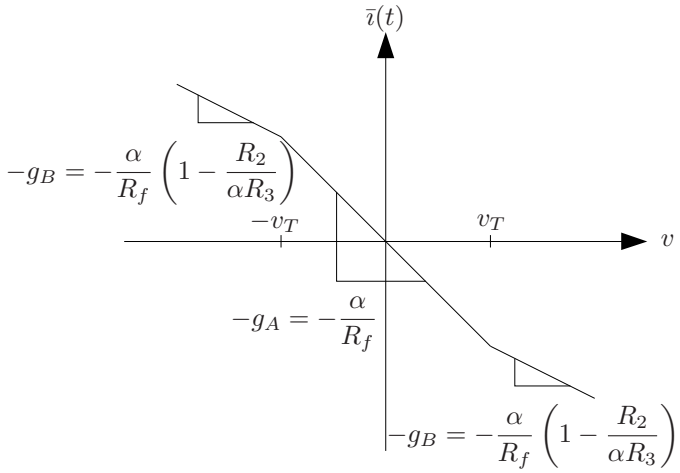

Figure 2.8. Current-voltage (i-v) characteristic of the piecewise-linear analog NRC with approximate slopes.

2.3.2 Sampled-Data Implementation

It is not straightforward to directly implement the dependent current source as a digital system, because DACs behave as voltage sources. Instead, this thesis creates a sampled-data NRC based on the circuit in Figure 2.5a with a dependent voltage source. Figure 2.9 shows the implementation, where the dependent voltage source is replaced by a sampled-data system. Denoting the sample period as T, the value of the terminal voltage $v(t)$ at the sample instance $t = kT$ is $v(k)$, where k is an integer. The lookup table (LUT) transforms the sampled input voltage to a sampled output voltage $v_1(kT)$. In turn, this voltage is converted to a analog voltage by a zero-order hold (ZOH) DAC such that

$$\overline{v}_1(t) = v_1(k) \qquad \text{for} \qquad kT \le t < (k+1)T. \tag{2.27}$$

The output waveform $\overline{v}_1(t)$ is a staircase signal that is used to approximate the i-v characteristic in Figure 2.5b. It follows from Eq. (2.16) that

$$\overline{\imath}(t) = \frac{v(t) - \overline{v}_1(t)}{R_f} = \frac{v(t) - v_1(k)}{R_f} \approx \frac{v(t) - \overline{G}(v)}{R_f}, \tag{2.28}$$

where $v_1(k) = \overline{G}(v)$ at time $t = kT$. Therefore, the signal $\overline{v}_1(t)$ is a staircase approximation of the analog signal $v_2(t)$ in Figure 2.7. However, because the LUT is used instead of an analog circuit, it is easy to implement arbitrary i-v characteristics.

The remaining two sections of the chapter describe performance parameters for a marginal oscillator. Section 2.4 shows how the i-v characteristics of the feedback function affect the conversion gain of the marginal oscillator. Section 2.5 defines sensitivity, noise factor, and noise figure for a marginal oscillator, which describe the characteristics of a marginal oscillator in the presence of noise.

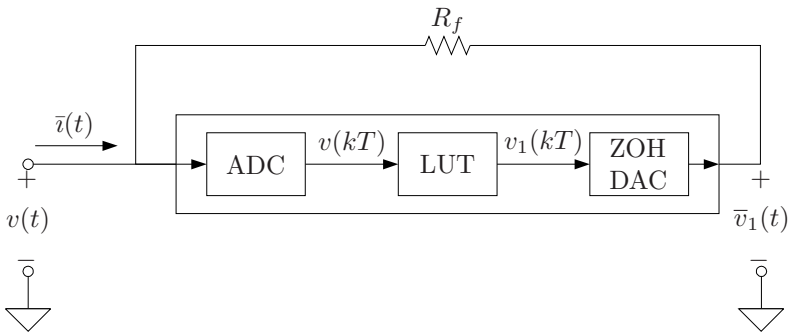

Figure 2.9. Sampled-data NRC.

2.4 Conversion Gain

The conversion gain is the sensitivity of the oscillation amplitude with respect to losses in the resonant circuit and is defined as

$$G_c \equiv \frac{R}{A}\frac{\partial A}{\partial R}. \tag{2.29}$$

As discussed in Section 1.3, the conversion gain of a Q-meter is unity. A high conversion gain is desirable, because a small change in the losses of the resonant circuit is easily discernible by a larger change in the amplitude of the oscillation. A conversion gain much higher than unity, on the order 10 to 100, can be achieved with a marginal oscillator by choosing an appropriate nonlinear $G(v)$.

Viswanathan was the first researcher to calculate the conversion gain of a marginal oscillator. She considered the nonlinear feedback function $G(v)$ shown in Figure 2.3b. The conversion gain for the marginal oscillator with that feedback was determined by Viswanathan to be [12]

$$G_c = \frac{\pi}{2(1 - g_B/g_A)g_A R \sin\theta}, \tag{2.30}$$

where the angle $0 \leq \theta \leq \pi/2$ satisfies

$$\sin 2\theta + 2\theta = \frac{\pi}{1 - g_B/g_A}\left(\frac{1}{g_A R} - \frac{g_B}{g_A}\right). \tag{2.31}$$

This angle also relates oscillation amplitude A to the threshold voltage v_T defined in Figure 2.3b by

$$v_T = A \sin\theta. \tag{2.32}$$

When $g_A R$ is sufficiently greater than unity, the conversion gain depends only on $g_B R$. This limit is given by

$$\lim_{g_A R \to \infty} G_c = \lim_{\theta \to \infty}\left[\frac{1}{2}\left(\frac{\sin 2\theta + \sin\theta}{\sin 2\theta}\right)\frac{1}{1 - g_B R}\right] = \frac{1}{1 - g_B R}. \tag{2.33}$$

For a hard limiter with $g_B = 0$ and a sufficiently large $g_A R$, the conversion gain is unity.

Given a marginal oscillator with given values of R, L, and C, it is necessary to determine g_A, g_B, and v_T to obtain an amplitude A and a conversion gain G_c. Unfortunately, in the three Eqs. (2.30) through (2.32), A and G_c are known, while g_A, g_B, v_T, and θ are unknown. To obtain a solution, first choose g_A so that $g_A R$ is slightly greater than unity, as required for oscillation. Given A, G_c, and $g_A R$, it is possible to solve for θ using Eqs. (2.30) and (2.31). First, solve Eq. (2.30) for g_B/g_A,

$$\frac{g_B}{g_A} = 1 - \frac{\pi}{2G_c g_A R \sin\theta}. \tag{2.34}$$

Substitute Eq. (2.34) into Eq. (2.31) to get

$$\pi = 2\theta + (1 + 2G_c(g_A R - 1)) \sin 2\theta. \tag{2.35}$$

The latter equation can be solved for θ, where $\theta \in [0, \pi/2]$. Once θ is obtained, g_B can be found by using Eq. (2.30),

$$g_B = g_A - \frac{\pi}{2RG_c \sin 2\theta}. \tag{2.36}$$

Finally, knowledge of θ and A allows the calculation of the threshold voltage using Eq. (2.32).

2.5 Sensitivity and Noise Figure

Before sensitivity and noise figure can be discussed, the effect of noise as well as the SNR of a marginal oscillator and a Q-meter need to be defined. This thesis assumes that all of the noise is due to thermal noise in the resistance R of the resonant circuit. Thermal noise is assumed to be Gaussian white noise with a power spectral density (PSD) of [16]

$$S_n(\omega) \cong 2kT \text{ watts per Hz} \qquad \text{for} \qquad |\omega| \ll 2\pi kT/h, \tag{2.37}$$

where T is the temperature of the conducting medium in Kelvin, k is Boltzmann's constant, and h is Planck's constant. Figure 2.10 shows that the thermal noise of the resistance R is modeled

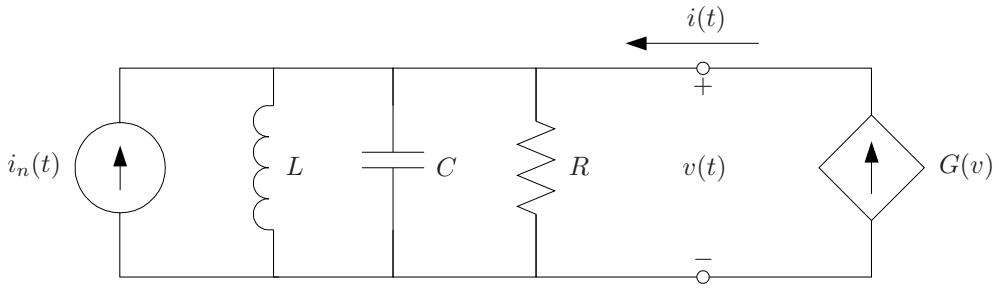

Figure 2.10. Schematic representation of a marginal oscillator with addition of thermal noise.

as a current source $i_n(t)$ in parallel with R, with a PSD of

$$S_i(\omega) = \frac{2kT}{R}. \tag{2.38}$$

The SNR of a marginal oscillator as well as that of a Q-meter is defined as the ratio of the rms envelope voltage due to changes in the losses of the resonant circuit to the rms envelope voltage due to thermal noise.

First consider the Q-meter system shown in Figure 2.11. As the independent current source $i(t)$ is noiseless, only the current source $i_n(t)$ contributes to the noise of the envelope of $v(t)$. From Eq. (2.9), the transfer function that relates the noise current $i_n(t)$ to the voltage $v(t)$ is

$$H(j\omega) = \frac{\frac{1}{C}j\omega}{(j\omega)^2 + \frac{\omega_n}{Q}j\omega + \omega_n^2}. \tag{2.39}$$

Assuming the rms value of the independent current signal is much larger than the rms value of the noise signal, it can be shown that the mean-square value of the envelope of $v(t)$ due to the noise source $i_n(t)$ is [17]

$$v_{rms}^2 = \frac{1}{2\pi}\int_{-\infty}^{\infty} S_v(\omega)\, d\omega, \tag{2.40}$$

where

$$S_v(\omega) = |H(j\omega)|^2 S_i(\omega). \tag{2.41}$$

Stremeler shows that Eq. (2.40) can be expressed equivalently as [16]

$$v_{rms}^2 = \frac{1}{\pi}|H(j\omega_0)|^2 S_i(\omega) B_{eq} = \frac{1}{\pi}R^2\frac{2kT}{R}\frac{\pi}{2RC} = \frac{kT}{C}, \tag{2.42}$$

where $|H(j\omega_0)|^2 = R^2$ is the midband system voltage gain and

$$B_{eq} = \frac{\pi}{2RC} \text{ rad/s} \tag{2.43}$$

is the equivalent bandwidth, as derived in Appendix A. It follows from Eq. (2.42) that the rms

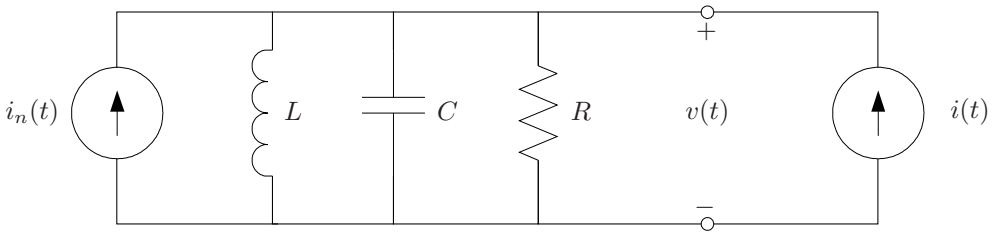

Figure 2.11. Schematic representation of a Q-meter with addition of thermal noise.

envelope noise is

$$v_{rms} = \sqrt{\frac{kT}{C}}. \tag{2.44}$$

Note that the rms envelope noise is independent of the resistance R. This is because even though the PSD of the noise current is inversely proportional to R, the bandwidth of the resonant circuit is proportional to R. These two effects cancel, yielding the above result.

Because the conversion gain of a Q-meter is unity, a change in the losses causes a proportionally equal change in the envelope voltage. For a change in the losses ΔR, the change in the rms amplitude is

$$\Delta A_{rms} = \frac{\Delta R}{R} A_{rms} = \xi A_{rms}. \tag{2.45}$$

Therefore, the SNR of a Q-meter is

$$\mathrm{SNR}_{\text{Q-meter}} = \frac{\Delta A_{rms}}{v_{rms}} = \xi A_{rms} \sqrt{\frac{C}{kT}}, \tag{2.46}$$

where ξ is the normalized change in the losses $\Delta R/R$.

In a marginal oscillator, because of the nonlinear feedback element, the rms noise is also effected by the form of $G(v)$. Viswanathan gives the rms noise of the marginal oscillator as [12]

$$v_{rms} = \sqrt{\frac{kTG_c}{C}}. \tag{2.47}$$

The conversion gain G_c of a marginal oscillator indicates that a change in the losses causes a change in the envelope voltage that is proportionally G_c times as much. Therefore, for a change in the losses ΔR, the change in the rms amplitude is

$$\Delta A_{rms} = \frac{\Delta R}{R} G_c A_{rms} = \xi G_c A_{rms}. \tag{2.48}$$

This means the SNR of a marginal oscillator is

$$\mathrm{SNR}_{\text{m.o.}} = \frac{\Delta A_{rms}}{v_{rms}} = \xi A_{rms} \sqrt{\frac{CG_c}{kT}}. \tag{2.49}$$

This thesis defines the sensitivity of a marginal oscillator as the change in the normalized change in the losses $\xi = \Delta R/R$ that leads to a unity SNR in the presence of thermal noise. It follows that the sensitivity is

$$S_{\text{m.o.}} = \xi = \frac{1}{A_{rms}} \sqrt{\frac{kT}{CG_c}}, \tag{2.50}$$

Notice that increasing the conversion gain causes the value of the sensitivity to decrease.

This thesis defines the NF as

$$\mathrm{NF} = \frac{\mathrm{SNR}_{\text{Q-meter}}}{\mathrm{SNR}_{\text{m.o.}}}. \tag{2.51}$$

Using this definition, the NF of a marginal oscillator is

$$\mathrm{NF} = \frac{1}{\sqrt{G_c}}. \tag{2.52}$$

The noise figure, $10\log_{10}(\mathrm{NF})$, is

$$\text{noise figure} = -5\log_{10}(G_c). \tag{2.53}$$

Typically, conversion gains are greater than unity, so the NF of a marginal oscillator is less than unity. This is different from the NF of an amplifier, which is never less than unity. This indicates that as the conversion gain increases, the effect of thermal noise on the output voltage of the envelope decreases.

Chapter 3

Simulations

The marginal oscillator is simulated using Simulink, a simulation tool in MATLAB. Within Simulink, the marginal oscillator is represented by the all-integrator block diagram in Figure 3.1. Performing the simulation using an m-file exclusively is undesirable, because a necessary function call leads to significantly longer simulation times.

3.1 Marginal Oscillator Parameter Values

Numerical simulations in this study use circuit values of an experimental marginal oscillator. For this system, the nominal frequency of oscillation $f_n = 3.308$ MHz is obtained using an inductance $\overline{L}$ of 22.8 μH and a capacitance $\overline{C}$ of 101.53 pF. The losses of the resonant circuit are established from measurements of the system 3 dB bandwidth obtained using a vector network analyzer.

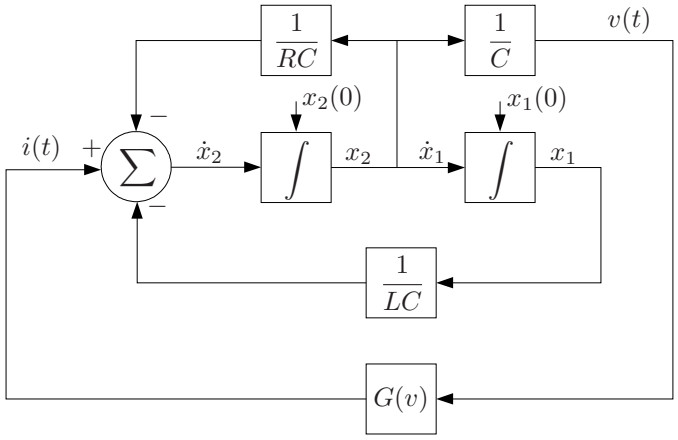

Figure 3.1. Block diagram of marginal oscillator.

Using Eq. (2.8), the nominal Q-factor of the resonant circuit is

$$\overline{Q} = \frac{f_n}{3 \text{ dB BW}} = \frac{3.308 \text{ MHz}}{26.464 \text{ kHz}} = 125.0. \tag{3.1}$$

Using Eq. (2.8), it follows that the nominal losses of the resonant circuit is

$$\overline{R} = Q\omega_n L = 59.237 \text{ k}\Omega. \tag{3.2}$$

The experiment is designed with a fixed value of g_A chosen so that $g_A R = 1.0344$. It follows that the nominal value of g_A is

$$\overline{g}_A = \frac{1.0344}{\overline{R}} = 17.462 \ \mu\mho. \tag{3.3}$$

The nominal values $\overline{L}$, $\overline{C}$, $\overline{R}$, and $\overline{g}_A$ will be used in subsequent simulations.

In practice, given $\overline{L}$, $\overline{C}$, $\overline{R}$, and $\overline{g}_A$, the user then specifies the conversion gain G_c and the amplitude A, and then solves for g_B and v_T using Eqs. (2.32), (2.35), and (2.36). In particular, given G_c and $g_A R$, Eq. (2.35) is solved for θ. Once θ is known, g_B is found using Eq. (2.36), and v_T is found using Eq. (2.32). This study uses a conversion gain G_c of 10 and a nominal amplitude $\overline{A}$ of 0.25 V. This results in $\overline{g}_B = 14.795 \ \mu\mho$ and $\overline{v}_T = 0.1670$ V.

Additional necessary parameters are the initial values $x_1(0)$ and $x_2(0)$ of the integrator outputs. To derive these values, suppose the voltage has the form

$$v(t) = a\cos(\omega t), \tag{3.4}$$

with $a > 0$. This means the initial conditions on the voltage are $v(0) = a$ and $\dot{v}(0) = 0$. From Eq. (2.13),

$$x_2(0) = Ca. \tag{3.5}$$

Now consider the inputs and output of the summation block in Figure 2.2,

$$\dot{x}_2(t) = i(t) - \frac{1}{RC}x_2(t) - \frac{1}{LC}x_1(t). \tag{3.6}$$

At time $t = 0$, this simplifies to

$$x_1(0) = LC\left[G(a) - \frac{a}{R}\right], \tag{3.7}$$

where

$$G(a) = \begin{cases} g_A a, & a < v_T \\ g_A v_T + (a - v_T)g_B, & \text{otherwise} \end{cases}. \tag{3.8}$$

If $a < v_T$, the initial conditions simplify to

$$x_1(0) = \frac{LCa}{R}(g_A R - 1) \tag{3.9}$$

$$x_2(0) = Ca. \tag{3.10}$$

This study chooses $a = 0.1$ V. It follows that $x_1(0) = 1.3442\times10^{-022}$ and $x_2(0) = 1.0153\times10^{-011}$.

Using simulations, we ultimately want to determine the conversion gain G_c. Using the approximation given by Miller [8],

$$G_c \approx \frac{\Delta A}{\Delta R}\frac{R}{A}, \tag{3.11}$$

where A is a function of R. This thesis shows that this expression is only valid if ΔR is small. To understand why this is true, it is useful to determine the oscillation amplitude A as a function of the losses R for a fixed conversion gain. As mentioned earlier, the nominal value of $g_A R$ is 1.0344. Given G_c and $g_A R$, Eq. (2.35) is then solved for θ. Once θ is known, g_B is determined using Eq. (2.36). The threshold voltage v_T is determined so that for the nominal value of $\overline{R} =$ 59.237 kΩ, the amplitude A is 1 V. As R is varied, the fixed values of g_A, g_B, and v_T are used. Figure 3.2 shows a plot of the amplitude A versus the losses R for conversion gains G_c of 10, 25, and 50. Note that for all curves, $A = 1$ V at $R = \overline{R}$ by design. Also note that as G_c gets larger, the curves become more nonlinear with respect to R. Therefore, the estimation of $\partial A/\partial R$ by $\Delta A/\Delta R$ must use a smaller ΔR as G_c increases.

The effect of the nonlinear relation between A and R on the approximation of G_c by Eq. (3.11) is now considered. Let

$$\widehat{G}_c = \frac{\Delta A}{\Delta R}\frac{\overline{R}}{\overline{A}} = \frac{\overline{A} - A}{\overline{R} - R}\frac{\overline{R}}{\overline{A}}, \tag{3.12}$$

where $\overline{A}$ and $\overline{R}$ represent the nominal amplitude of oscillation and losses, respectively. In order to obtain the estimate $\widehat{G}_c$, in experiment and simulation, the nominal losses $\overline{R}$ is perturbed by an amount ΔR using a calibration circuit [18]. When the calibration circuit is turned on, additional losses are introduced into the circuit so that

$$R = \overline{R} - \Delta R. \tag{3.13}$$

A decrease in the losses leads to a decrease ΔA in A so that

$$A = \overline{A} - \Delta A. \tag{3.14}$$

The question arises as to how small ΔR must be so that $\widehat{G}_c$ is a good estimate of G_c. To determine this, $\widehat{G}_c$ is calculated as a function of ΔR using Eq. (3.12). More specifically, using the $\overline{R}$ specified above, $\overline{A} = 1$ V, and $G_c = 25$, the amplitude A is calculated as a function of R using the procedure that generated Figure 3.2, and the estimate $\widehat{G}_c$ is calculated using Eq. (3.12). Figure 3.3 shows the estimated conversion gain $\widehat{G}_c$ versus $\Delta R/R$. The estimated conversion gain quickly diverges away from the actual conversion gain as ΔR is increased. From the figure, for $\Delta R/R$ of approximately 0.5%, $\widehat{G}_c$ is at 90% of G_c.

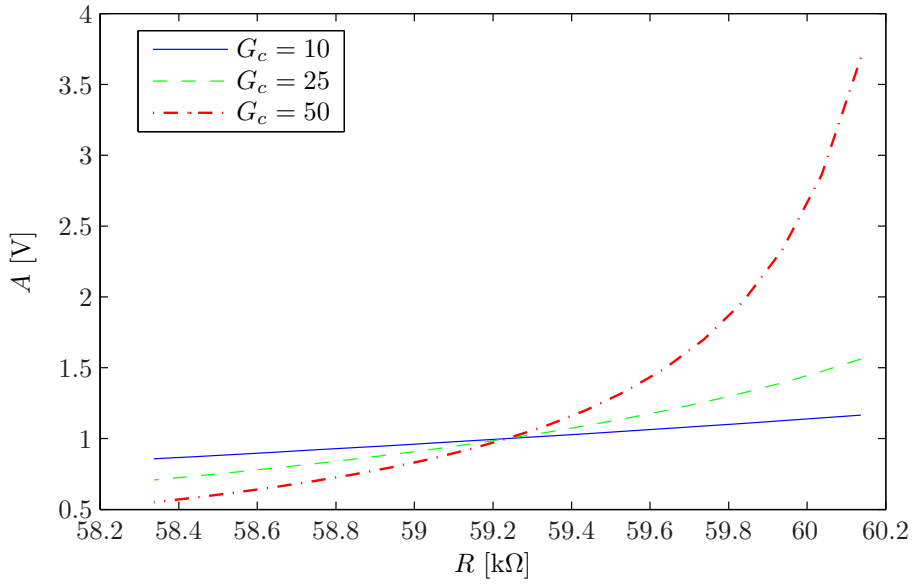

Figure 3.2. Amplitude vs. Losses.

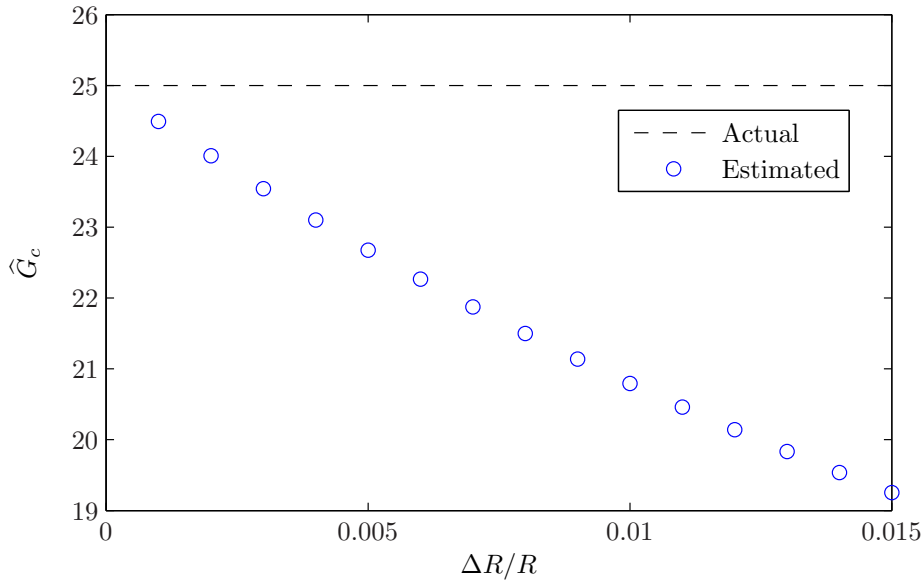

Figure 3.3. Conversion Gain vs. Change in Losses.

3.2 Solver and Integration Parameter Selection

In order to determine the appropriate solver, the concept of stiffness needs to be understood. The idea of stiffness originated fifty years ago when computers became available for widespread use in solving ODEs. It is not well known what makes a problem stiff. In fact, there exist many definitions of stiffness, such as:

- Systems containing very fast components as well as very slow components [19].
- Systems that represent coupled physical systems having components varying with very different times scales: that is they are systems having some components varying much more rapidly than the others [20].
- Stiff equations are equations where certain implicit methods perform better, usually tremendous better, than explicit ones [21].

Brugnano proposed a unified definition in which systems are stiff when the stiffness ratio,

$$\sigma_c = \frac{k_c}{\gamma_c} = \frac{\max\limits_{t\in[o,T]} |y(t)|}{\dfrac{1}{T}\displaystyle\int_0^T |y(t)|dt}, \tag{3.15}$$

is much greater than unity [22]. This definition is applicable to many scenarios as discussed by Brugnano. For oscillatory systems, such as the marginal oscillator, Brugnano showed that σ_c can be approximated as

$$\sigma_c = 2\pi\frac{T}{T^*}, \tag{3.16}$$

where T is the length of the simulation and T^* is the period of oscillation. In a marginal oscillator, the time constant for change in amplitude is given by Viswanathan as [12]

$$\tau = 2RCG_c. \tag{3.17}$$

For a typical application where $R = 60$ kΩ, $C = 100$ pF, and $G_c = 10$, $\tau = 1.2 \times 10^{-4}$ s. To observe changes in amplitude, set $T = 5\tau$. For oscillation at 3.3 MHz,

$$T^* = \frac{1}{3.3 \text{ MHz}} = 3.0303 \times 10^{-7} \text{ s}. \tag{3.18}$$

It follows that

$$\sigma_c = \frac{T}{T^*} = \frac{5\tau}{T^*} = 1980 \gg 1. \tag{3.19}$$

The marginal oscillator is stiff because $\sigma_c \gg 1$.

The marginal oscillator system is solved using the MATLAB ODE suite, a collection of codes for solving initial value problems given by first-order systems of ODEs. Functions in the ODE suite are categorized by how they choose the step-size and how they solve for the next value of the response. Fixed-step solvers provide a solution at points in time separated by a fixed interval, while variable-step solvers adjust the interval between solution points. Explicit solvers directly compute the next solution using known quantities, while implicit solvers find the next solution by solving a set of equations using an iterative technique.

Both fixed-step and variable-step solvers calculate the next simulation time by adding the current simulation time and the step size. For fixed-step solvers, the step size is constant and user-specified. For variable-step solvers, the step size is chosen by the solver to meet specified relative

and absolute error tolerances. The relative tolerance specifies the allowable error with respect to each state variable. The absolute tolerance represents the allowable error for state variable values close to zero. A variable-step solver is preferable, because it can significantly shorten the simulation time. This is because, for a given level of accuracy, the solver can dynamically adjusts the step size as necessary and thus reduce the number of steps.

Explicit solver calculate the values of the next state as a function of previous states and state derivatives. In contrast, implicit solvers find the next state by solving a coupled set of algebraic equations dependent on the next state derivative using a Newton-like method. The result of this approach is that implicit solvers provide greater stability for oscillatory behavior, like that found in stiff systems. However, they do so by sacrificing accuracy and are more computationally expensive. Therefore, implicit solvers are generally used for stiff systems, while explicit solvers are used for nonstiff systems.

The MATLAB ODE suite contains several solvers. The variable-step solvers are `ode23`, `ode45`, `ode113`, `ode15s`, `ode23s`, `ode23t`, and `ode23tb`. The fixed-step solvers are `ode1`, `ode2`, `ode3`, `ode4`, `ode5`, `ode8`, and `ode14x`. Of these solvers, `ode15s`, `ode23s`, `ode23t`, `ode23tb`, and `ode14x` are implicit, and the rest are explicit.

It is desirable to use a variable-step solver to reduce simulation time and memory usage. Out of the available variable-step solvers, this study chooses `ode15s` for two reasons. First, the ODE describing the marginal oscillator is very stiff. This means an implicit solver other than `ode23t`, which is only effective for moderately stiff systems [23], must be used. Second, a high level of accuracy is desired. This rules out `ode23s` and `ode23tb`, which are more effective at crude tolerances [24, 25].

The `ode15s` solver has several parameters. This thesis adjusts the relative and absolute tolerances to strike a balance between accuracy and simulation time. To determine the appropriate tolerances, simulations were conducted for several different tolerances, with a nominal amplitude $\overline{A}$ of 0.25 V, a change in losses ΔR of 47.389 Ω, and a desired conversion gain of 10. This study chooses the appropriate tolerances by comparing simulated and theoretical values of the estimated conversion gain $\widehat{G}_c$, the nominal amplitude $\overline{A}$, the new amplitude A from a change ΔR in the losses, the natural frequencies f_n at both amplitudes, and the time constants τ transitioning between the two amplitudes. In addition, the total simulation time is taken into account.

The simulated values are obtained using Simulink according to the following procedure. The Simulink model was first run for a total of 9.3 ms. With $R = \overline{R}$, the simulated voltage was given 2 ms to reach steady-state and is then observed for 1 ms. Then, the resistance is changed to $R = \overline{R} - \Delta R$ over 0.1 ms. At the new R, the voltage is again given 2 ms to reach steady-state and observed for 1 ms. Finally, the resistance is changed back to $R = \overline{R}$ over 0.1 ms, and the voltage is observed in the same manner as before. Then, the positive and negative peaks of the voltage are found. From this, it is possible to determine the envelope voltage as well as the oscillation frequency. The conversion gain can be estimated from the envelope voltage using Eq. (3.11). For the two transition regions, the corresponding rise or fall time is determined as the time it takes for the envelope voltage to transition between 10% and 90% of the difference between the two

steady-state values. From the rise and fall times, it is possible to calculate the time constants using $\tau = t_r/\ln 9$ and $\tau = t_f/\ln 9$, respectively. Table 3.1 compares theory with the simulation results, obtained using 64-bit Matlab R2010a on a Windows 7 computer with a Intel Core 2 Duo T9300 processor at 2.5 GHz and 4 GB of RAM. The simulation results are mostly consistent with theory except for the time constants τ. Therefore, the solver tolerances are chosen based on the simulated time constants and the simulation time. This study finds the best compromise between accuracy and speed is achieved with a relative tolerance of 10^{-10} and an absolute tolerance of 10^{-30}. This set of tolerances results in more accurate time constants compared with other sets with similar or shorter simulation times, while a more accurate set of tolerances needs nearly double the simulation time.

It is not always possible to use a variable-step solver. As described in Section 3.3, a fixed-step solver is sometimes necessary. Therefore, this study also determines the preferred fixed-step solver. While `ode14x` is the only implicit fixed-step solver, simulations show that the explicit solvers have comparable accuracy and much shorter simulation times. Therefore, all of the fixed-step solvers need to be considered. To determine the appropriate solver and step size, simulations were performed with the same procedure that produced Table 3.1 except that the simulations were done for different fixed-step solvers and step sizes. Table 3.2 shows the results of the simulations. As with the previous set of simulations, the simulation results are mostly consistent with theory except for the time constants τ. Therefore, the solver and step size are chosen based on the simulated time constants and the simulation time. Note that the accuracy of the simulations is largely determined by the step size for solvers of sufficiently high orders. Using a higher order solver than `ode4` does not result in greater accuracy, while using a lower order solver reduces accuracy. The simulated time constants for step sizes of 0.25 ns and 0.5 ns are both very close to theory, while those for larger step sizes are less accurate. Therefore, this study finds the best compromise between accuracy and speed is achieved with the `ode4` solver with a step size of 0.5 ns.

3.3 Thermal Noise

Thermal noise is of importance to marginal oscillator performance, because it sets the SNR of measurements. To better understand the effect of thermal noise, this section has three goals. The first goal is to incorporate thermal noise into the simulation model for the marginal oscillator. The second goal is to use simulation to verify the relationship between the noise factor (NF) and the conversion gain given in Eq. (2.52). For the third goal, it is well known that the SNR in pulsed quadrupole resonance spectroscopy varies as the square root of the coil Q-factor [26]. The coil Q-factor is usually on the order of 100. However, recent attempts at Penn State by Pusateri have resulted in high-temperature superconductor coils with Q-factors on the order of 500,000. The third goal is to verify using simulation whether this relationship still exists for very high Q-factors.

This thesis assumes the thermal noise is Gaussian white noise. However, simulation of ideal-

Table 3.1. Comparison of `ode15s` solver parameters.

Tolerance		$\widehat{G}_c$	$\overline{A}$ [V]	A [V]	f_n [Hz]		τ [μs]		Sim. Time [s]
rel.	abs.				$\overline{A}$	A	$\overline{A}$ to A	A to $\overline{A}$	
10^{-7}	10^{-18}	10.094	0.2498489	0.2478312	3308001	3308003	123.687	887.399	37.363
10^{-7}	10^{-20}	9.965	0.2498905	0.2478985	3307999	3307998	147.761	122.035	44.974
10^{-7}	10^{-26}	9.949	0.2498416	0.2478524	3308002	3307996	143.497	148.450	40.878
10^{-7}	10^{-30}	9.943	0.2498418	0.2478544	3308008	3308002	139.370	144.116	39.683
10^{-10}	10^{-18}	10.008	0.2498551	0.2478538	3308011	3307996	132.078	172.389	39.154
10^{-10}	10^{-20}	9.981	0.2499859	0.2479893	3308004	3307996	124.029	125.749	92.578
10^{-10}	10^{-26}	9.967	0.2499935	0.2480003	3308001	3307999	121.415	122.447	126.156
10^{-10}	10^{-30}	9.944	0.2499947	0.2480059	3308001	3308000	120.315	121.760	119.422
10^{-12}	10^{-20}	9.983	0.2499856	0.2479893	3308000	3308004	123.342	125.336	93.324
10^{-12}	10^{-30}	9.951	0.2499977	0.2480074	3308000	3308000	120.040	120.796	229.836
10^{-13}	10^{-30}	9.961	0.2499994	0.2480072	3308000	3307999	119.971	120.728	309.276
Theoretical		9.961	0.25	0.2480079	3308000		120.105	120.280	—

Table 3.2. Comparison of fixed-step solvers.

Solver	Step size [ns]	$\widehat{G}_c$	$\overline{A}$ [V]	A [V]	f_n [Hz]		τ [μs]		Sim. Time [s]
					$\overline{A}$	A	$\overline{A}$ to A	A to $\overline{A}$	
`ode3`	1	9.959	0.2497618	0.2477719	3308000	3308000	121.003	121.003	43.096
`ode3`	0.5	9.960	0.2499696	0.2479778	3308000	3308000	120.109	120.590	89.528
`ode3`	0.25	9.961	0.2499961	0.2480040	3308000	3308000	119.971	120.315	110.124
`ode4`	2	9.961	0.2499815	0.2479895	3308003	3307996	125.819	130.015	23.710
`ode4`	1	9.961	0.2499955	0.2480034	3308000	3308003	120.934	122.034	53.779
`ode4`	0.5	9.961	0.2499989	0.2480068	3308000	3308000	120.109	120.590	97.932
`ode4`	0.25	9.961	0.2499997	0.2480076	3308000	3308000	119.971	120.315	133.746
`ode5`	2	9.961	0.2499820	0.2479900	3308003	3307996	125.337	129.189	31.976
`ode5`	1	9.961	0.2499955	0.2480034	3308000	3308003	121.003	122.516	66.565
`ode5`	0.5	9.961	0.2499989	0.2480068	3308000	3308000	120.109	120.590	127.68
`ode5`	0.25	9.961	0.2499997	0.2480076	3308000	3308000	119.971	120.315	180.811
`ode8`	10	9.961	0.2495502	0.2475617	3307996	3307996	909.966	909.966	12.200
`ode8`	5	9.961	0.2498875	0.2478963	3307996	3307996	168.126	907.074	23.658
`ode8`	2	9.961	0.2499820	0.2479900	3308003	3307996	125.337	129.189	62.708
`ode8`	1	9.961	0.2499955	0.2480034	3308000	3308003	121.003	122.516	123.301
`ode8`	0.5	9.961	0.2499989	0.2480068	3308000	3308000	120.109	120.590	220.891
`ode14x`	10	9.961	0.2495798	0.2475910	3307996	3307996	909.966	909.893	99.773
`ode14x`	5	9.961	0.2498885	0.2478972	3307996	3307996	169.020	905.010	197.069
Theoretical		9.961	0.25	0.2480079	3308000		120.105	120.280	—

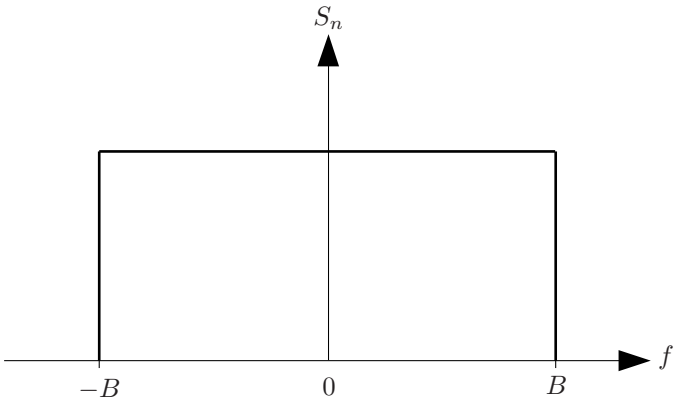

Figure 3.4. PSD of band-limited white noise.

ized white noise with a constant PSD is impossible, so band-limited white noise is used instead. To produce band-limited white noise, a fixed-step solver must be used. To see why, consider the PSD of band-limited white noise shown in Figure 3.4, which is nonzero for $-B < f < B$. This PSD leads to an autocorrelation described by a sinc function with zero crossings at $t = kT$, where $T = 1/2B$ and k is a nonzero integer. At a fixed sample rate of T, sampled values of band-limited Gaussian white noise are uncorrelated and independent in the Gaussian case. Hence, band-limited Gaussian white noise can be simulated using an independent and identically-distributed sequence of Gaussian random variables if the sample rate is fixed, as is the case with a fixed-step solver. Therefore, this thesis uses the fixed-step solver `ode4` with a step size of $T = 0.5$ ns for the reasons described in Section 3.2.

The band-limited Gaussian white noise is simulated using a Gaussian random number generator with a mean of zero and a variance of [16]

$$\sigma^2 = \frac{4kTB}{R}, \tag{3.20}$$

where k is Boltzmann's constant, T is the temperature in Kelvin, B is the bandwidth of the system, and R is the losses of the resonant circuit. The standard noise temperature of $T = 290$ K is used. The bandwidth is $B = 1/2T = 1$ GHz. Figure 3.5 shows the addition of the Gaussian random number generator that produces band-limited Gaussian white noise, represented by GWN, into the block diagram of the marginal oscillator.

This study considers the effect of thermal noise on the envelope of the voltage. To simplify simulations, only the steady-state envelope is considered. To do so, set the initial amplitude $a = \overline{A}$. The simulations were run for Q-factors ranging from order of magnitudes of zero to six and conversion gains of 1, 2, 5, 10, 25, 50, 100, 500, 1000, and 10^6. For each Q-factor and conversion gain G_c, it is possible to calculate the resistance R using Eq. (2.8) and the angle θ using Eq. (2.35). As mentioned before, the nominal value of $g_A R$ is 1.0344. It follows that $g_A = 1.0344/R$. Knowledge of G_c, R, g_A, and θ allows v_T and g_B to be found using Eqs. (2.32) and (2.36), respectively. For each combination of Q-factor and conversion gain, the

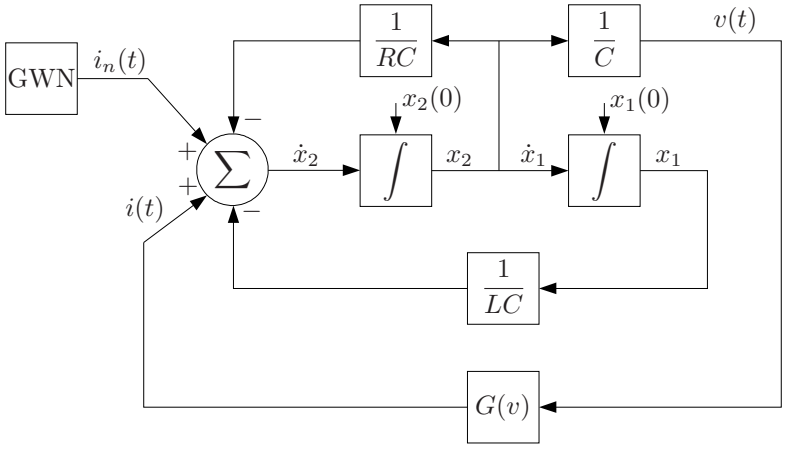

Figure 3.5. Block diagram of marginal oscillator with addition of Gaussian white noise block.

Table 3.3. Theoretical and simulated effects of thermal noise on rms envelope voltage in μV.

G_c	Theory	Simulation						
		$Q=1$	10	10^2	10^3	10^4	10^5	10^6
1	6.28	6.18	6.33	6.23	6.32	6.20	2.62	0.83
2	8.88	8.87	8.92	8.74	9.23	7.52	2.60	0.84
5	14.04	14.32	13.92	13.89	14.90	8.33	2.62	0.84
10	19.86	20.11	19.50	19.98	19.61	8.29	2.63	0.84
25	31.40	31.80	30.78	33.02	24.81	8.24	2.64	0.84
50	44.41	45.25	43.90	47.13	26.33	8.28	2.65	0.84
100	62.80	62.23	63.19	62.03	26.23	8.32	2.65	0.84
500	140.42	138.73	149.05	83.27	26.18	8.38	2.65	0.84
1000	198.59	199.84	196.15	82.94	26.32	8.39	2.65	0.84
10^6	6279.91	832.56	265.19	83.93	26.54	8.39	2.65	0.84

system is simulated twice, once with noise and once without, each time for 10 μs. The two envelope voltages are then calculated. The rms envelope voltage is then found by taking the standard deviation of the difference between the two enevelope voltages. The simulation results are shown in Table 3.3. Viswanathan predicts that the rms envelope noise given by Eq. (2.47) is proportional to the square root of G_c and independent of the Q-factor. However, simulation shows that the amount of noise is also affected by the Q-factor. To investigate the effect of the Q-factor on the rms envelope noise, it is useful to consider the plot of rms envelope noise versus Q-factor in Figure 3.6. In particular, consider the curve corresponding to a conversion gain of 10^6. It can be seen that the marginal oscillator limits the maximum rms envelope noise, and this limit is inversely proportional to the square root of the Q-factor. This makes sense, because the Q-factor is inversely proportional to the bandwidth of the resonant circuit. Thus, increasing the Q-factor decreases the bandwidth, resulting in decreased rms envelope noise. For significantly small Q-factor and conversion gain, for which the rms envelope noise is not limited, theory and simulation are in agreement.

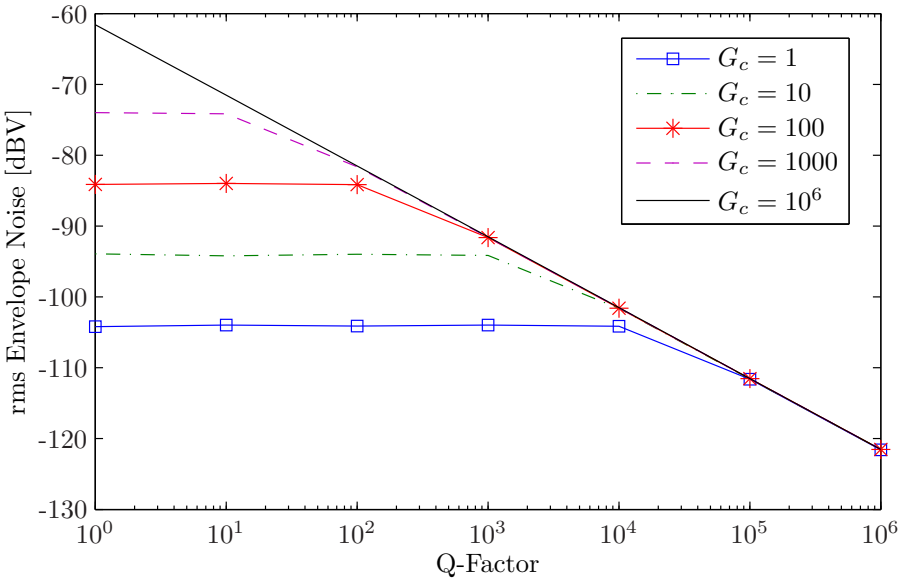

Figure 3.6. rms Envelope Noise versus Q-Factor.

It is useful to compare the NF for theory and simulation. Theory predicts that the NF given by Eq. (2.52) is inversely proportional to the square root of G_c. Using Eq. (2.51), the NF from simulation can be computed as

$$\mathrm{NF} = \frac{\mathrm{SNR}_{\text{Q-meter}}}{\mathrm{SNR}_{\text{m.o.}}} = \frac{\Delta A_{rms,\text{Q-meter}}/v_{rms,\text{Q-meter}}}{\Delta A_{rms,\text{m.o.}}/v_{rms,\text{m.o.}}}, \tag{3.21}$$

where ΔA_{rms} is the change in rms amplitude from a change ΔR in the losses and v_{rms} is the rms envelope noise. Using the conversion gain approximation in Eq. (3.11) and the fact that the conversion gain of a Q-meter is unity, it follows that

$$\mathrm{NF} = \frac{(A/\sqrt{2})(\Delta R/R)}{G_c(A/\sqrt{2})(\Delta R/R)} \frac{v_{rms,\text{m.o.}}}{v_{rms,\text{Q-meter}}} = \frac{v_{rms,\text{m.o.}}}{G_c v_{rms,\text{Q-meter}}}. \tag{3.22}$$

It has already been shown that for sufficiently small Q-factors, the rms envelope noise for the marginal oscillator is directly proportional to the square root of G_c. Because the rms envelope noise for the Q-meter is a constant, it follows that the NF is inversely proportional to the square root of G_c, as predicted by theory.

It is also useful to determine the effect of the Q-factor on the SNR of the marginal oscillator using simulation. The SNR of the marginal oscillator as defined Section 2.5 is

$$\mathrm{SNR}_{\text{m.o.}} = \frac{\Delta A_{rms}}{v_{rms}}, \tag{3.23}$$

where ΔA_{rms} is the change in rms amplitude from a change ΔR in the losses, independent of the Q-factor, and v_{rms} is the rms envelope noise. As determined above, for sufficiently large

Table 3.4. Effect of a sampled-time NRC.

f_s [MHz]	$\widehat{G}_c$	$\overline{A}$ [V]	A [V]	f_n [Hz]		τ [μs]	
				$\overline{A}$	A	$\overline{A}$ to A	A to $\overline{A}$
≤ 46	Does Not Oscillate						
47	25.670	0.1724287	0.1688877	3305029	3305026	372.768	277.407
50	13.838	0.1834444	0.1814137	3305213	3305210	171.021	165.995
75	10.177	0.2197864	0.2179970	3306155	3306154	123.205	124.581
100	9.990	0.2326172	0.2307581	3306621	3306618	120.986	121.674
200	9.950	0.2455382	0.2435836	3307311	3307311	119.928	121.510
500	9.958	0.2492712	0.2472855	3307726	3307725	120.463	122.870
1000	9.981	0.2498045	0.2478142	3307863	3307863	120.182	120.939
Continuous	9.944	0.2499947	0.2480059	3308001	3308000	120.315	121.760

Q-factors, the rms envelope voltage is inversely proportional to the square root of the Q-factor. It follows that the SNR of the marginal oscillator varies with the square root of the Q-factor.

3.4 Sampled-Time Implementation

Realizing a NRC with even a simple i-v characteristic as shown in Figure 2.3b is not an easy task using analog circuits. To simplify the hardware representation of the NRC, it is useful to implement the NRC using a sampled-data system. This thesis seeks to ultimately show the feasibility of implementing the NRC using a sampled-data system. As a first step, this study investigates implementing the NRC using a sampled-time system, where time is quantized but amplitude is not. To more closely match the sampled-data implementation given in Section 2.3.2, the NRC in the simulation is implemented as the current

$$i(t) = \frac{\overline{G}(v(kT)) - v(t)}{R_f} \qquad \text{for} \qquad kT \leq t < (k+1)T, \tag{3.24}$$

where $T = 1/f_s$, the sample period, is equal to the inverse of the sample rate f_s. This implementation is similar to the implementation in Figure 2.5a except that $\overline{G}(v)$ is now quantized in time. Figure 3.7 shows the marginal oscillator block diagram with this sampled-time implementation of the NRC. The simulations were performed for different sample rates using the same procedure that generated Table 3.1. The feedback resistance R_f is 100 Ω for the simulations. Table 3.4 shows the effect of different sample rates f_s on marginal oscillator performance. Simulation reveals that a minimum sample rate of 47 MHz is necessary to achieve oscillation. As the sample rate increases, the results more closely match the continuous results. Namely, as the sample rate increases, the conversion gain decreases, the oscillation amplitudes increase, the oscillation frequencies increase, and the time constants decrease. It is interesting to note that the conversion gain increases when the NRC is sampled. This reveals the possibility of using quantization of the NRC in time in order to increase the conversion gain.

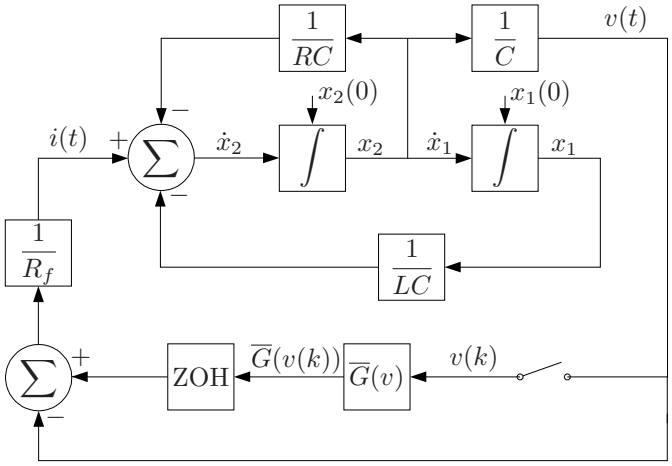

Figure 3.7. Block diagram of marginal oscillator with sampled-time NRC.

3.5 Sampled-Data Implementation

Having determined the sample rate needed for the marginal oscillator to function, this study investigates the effect of implementing the NRC using a sampled-data system, where amplitude is quantized in addition to time. To do so, a quantizer is added before the input to $\overline{G}(v)$ in Figure 3.7. The resulting marginal oscillator with a sampled-data implementation of the NRC is shown in Figure 3.8. As before, the resistance R' is fixed at 100 Ω. The quantizer calculates the output based on the input such that

$$y = q \times \text{round}\left(\frac{u}{q}\right), \tag{3.25}$$

where y is the output, u is the input, and q is the quantization interval. It is convenient to relate the quantization interval q to the number of quantization bits N by

$$q = \frac{2v_{max}}{2^N}, \tag{3.26}$$

where the v_{max} is the maximum output of the quantizer and $-v_{max}$ is the minimum. This study chooses $v_{max} = 5$ V. The simulations use with a sample rate of 100 MHz, which produces good results and is achievable with current technology. The same procedure as in Section 3.4 is used for the simulations. Table 3.5 shows the simulation results of the effect of quantization in both time and amplitude on the performance of a marginal oscillator. The results show that a quantizer resolution of 10 bits and a sample rate of 100 MHz is sufficient to achieve the desired conversion gain. However, a higher resolution of 12 bits lowers the time constant, which is useful to reduce the necessary measurement time. Any additional increase in resolution has minimal effect on the performance of the marginal oscillator.

In a physical implementation of the NRC by a discrete-time DSP system, such as shown in Figure 2.9, the output of the NRC would be delayed. Delays of 100 ns can be expected

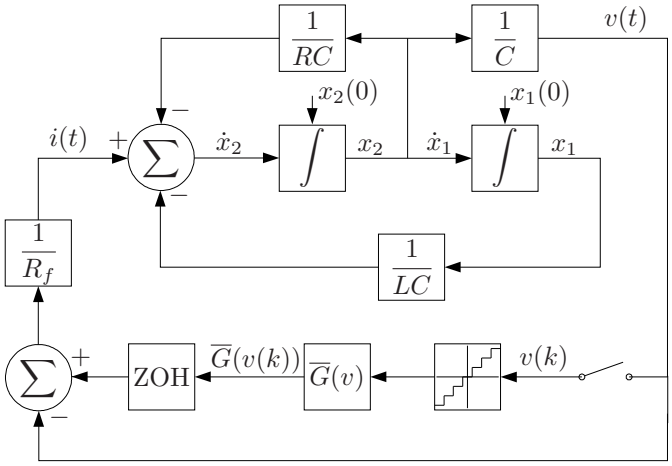

Figure 3.8. Block diagram of marginal oscillator with sampled-data NRC.

with current technology. Keeping in mind that the nominal oscillation period $T_n = 1/f_n$ is 302.3 ns, a delay that is a third of the oscillation period could negatively impact the oscillation of the marginal oscillator. Therefore, the effect of a delayed NRC output on marginal oscillator performance is investigated. Consider the marginal oscillator block diagram in Figure 3.9, where the output sampled-data NRC is delayed by a time d. The marginal oscillator was simulated with a sample rate of 100 MHz and 14 bits of quantization for several different delay values. The simulation results are shown in Table 3.6. Small delays less than or equal to 6 ns allow the marginal oscillator to still oscillate. The delay of 6 ns corresponds to approximately 7° of phase delay at the nominal frequency. A delay of 100 ns, which corresponds to 119° of phase delay, would cause the marginal oscillator to not function. However, delays close to a multiple of the oscillation period also allow oscillation without too much impact on the conversion gain. This result reveals the feasibility of a physical implementation of a marginal oscillator with a sampled-data NRC by increasing the delay to a multiple of the oscillation period.

Another method of allowing the marginal oscillator to still oscillate is to implement larger gains in the feedback path to counter the loss of amplitude that results from a large NRC output delay. This thesis implements the larger gains by determining the gains g_A and g_B as above, and then, increasing them by a gain factor α slightly larger than unity. The new gains are given by αg_A and αg_B, respectively. Tables 3.7 and 3.8 show the simulation results for various gain factors α for delays of 10 ns and 20 ns. The results show that increasing the gain in the feedback path can cause the marginal oscillator to function for larger delays, but the resulting oscillation frequency is lowered. Therefore, the effect of large delays can be mitigated by choosing appropriate gain factors.

Table 3.5. Effect of a sampled-data NRC with a sample rate of 100 MHz.

Quant. [bits]	G_c	$\overline{A}$ [V]	A [V]	f_n [Hz]		τ [μs]	
				$\overline{A}$	A	$\overline{A}$ to A	A to $\overline{A}$
≤ 5			Does Not Oscillate				
6	0.989	0.1222574	0.1221607	3306613	3306612	910.002	910.002
7	2.826	0.2200098	0.2195124	3306611	3306615	40.535	46.385
8	4.599	0.2325667	0.2317113	3306618	3306613	38.195	57.603
10	10.142	0.2323189	0.2304322	3306620	3306621	462.537	82.584
12	10.047	0.2326442	0.2307743	3306620	3306618	122.775	139.361
14	9.988	0.2326200	0.2307613	3306620	3306618	119.747	124.014
16	9.989	0.2326176	0.2307588	3306620	3306618	120.986	121.674
No Quant.	9.990	0.2326172	0.2307581	3306621	3306618	120.986	121.674

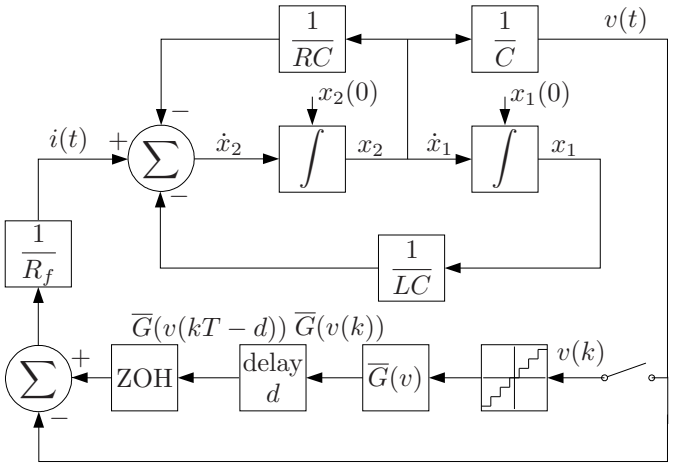

Figure 3.9. Block diagram of marginal oscillator with delayed sampled-data NRC.

Table 3.6. Effect of a sampled-data NRC with a sample rate of 100 MHz and 14 bits of quantization.

Delay [ns]	G_c	$\overline{A}$ [V]	A [V]	f_n [Hz]		τ [μs]	
				$\overline{A}$	A	$\overline{A}$ to A	A to $\overline{A}$
0	9.988	0.2326200	0.2307613	3306620	3306618	119.747	124.014
1	9.297	0.2271184	0.2249508	3306343	3306341	885.645	118.656
2	10.202	0.2203419	0.2185433	3306063	3306062	888.542	63.532
5	11.092	0.1955716	0.1937776	3316213	3316213	872.041	53.978
6	13.587	0.1852133	0.1832001	3307927	3307925	884.373	96.328
≥ 7			Does Not Oscillate				
$T_n = 302.3$	7.688	0.2328011	0.2313692	3312655	3306654	126.421	137.360
$2T_n$	9.882	0.2337906	0.2319357	3306686	3310685	125.044	124.768
$3T_n$	9.945	0.2343103	0.2324458	3308717	3309717	128.552	129.172

Table 3.7. Effect of a sampled-data NRC with a sample rate of 100 MHz, 14 bits of quantization, 10 ns delay, and gain factor α.

α	G_c	$\overline{A}$ [V]	A [V]	f_n [Hz]		τ [μs]	
				$\overline{A}$	A	$\overline{A}$ to A	A to $\overline{A}$
1.03	6.61	0.2001323	0.1990731	3303743	3303740	98.361	71.498
1.05	9.873	0.2444268	0.2424963	3303743	3303740	85.138	125.985
1.0525	9.926	0.2503142	0.2483274	3303745	3303740	85.827	123.781
1.055	9.785	0.2562818	0.2542758	3303743	3303741	85.897	111.865
1.06	9.632	0.2684544	0.2663856	3303745	3303741	125.848	84.037
1.07	9.572	0.2957769	0.2935121	3303744	3303742	110.626	96.919

Table 3.8. Effect of a sampled-data NRC with a sample rate of 100 MHz, 14 bits of quantization, 20 ns delay, and gain factor α.

α	G_c	$\overline{A}$ [V]	A [V]	f_n [Hz]		τ [μs]	
				$\overline{A}$	A	$\overline{A}$ to A	A to $\overline{A}$
1.15	9.926	0.2427437	0.2408161	3300457	3300459	99.70	101.361
1.1525	9.976	0.2482500	0.2462688	3300460	3300452	95.500	155.694
1.1535	9.752	0.2503422	0.2483889	3300459	3300452	89.984	129.838
1.155	6.526	0.2530491	0.2517377	3300458	3300453	106.119	77.504
1.17	9.841	0.2892584	0.2869815	3300461	3300457	106.327	190.929
1.2	12.414	0.3835295	0.3797176	3300459	3300453	164.524	147.908

Chapter 4

Discussion

4.1 Summary

This thesis accomplished its aims. First, it was verified that Viswanathan's theoretical predictions are correct through simulation. This was accomplished by choosing an appropriate solver and solver parameters, along with establishing a protocol for estimating conversion gain from simulation results. In addition, the theoretical predictions were also verified through experiment.

Second, it was shown through simulation that a sampled-data implementation of the NRC is feasible. This thesis was able to determine the minimum sample rate and quantization level that allows the marginal oscillator to properly function. It was also shown that the negative effect of a delayed NRC output due to the sampled-data implementation can be mitigated using larger gains on the feedback path or by increasing the delay to a multiple of the oscillation period.

Third, the effect of thermal noise on the marginal oscillator was taken into account. This thesis shows that Viswanathan's prediction of the rms envelope noise is inadequate and only correct for sufficiently small Q-factors.

4.2 Future Work

This thesis was able to predict several properties of the marginal oscillator using simulation. Further work in this area would need to experimentally verify the results. In addition, theory needs to be improved to describe the results seen.

Bibliography

[1] Roberts, A. (1947) "Two New Methods for Detecting Nuclear Radiofrequency Resonance Absorption," *Review of Scientific Instruments*, **18**(11), pp. 845–848.

[2] Rollin, B. V. (1949) "Nuclear paramagnetism," *Reports on Progress in Physics*, **12**(1), pp. 22–33.

[3] Pound, R. V. and W. D. Knight (1950) "A Radiofrequency Spectrograph and Simple Magnetic-Field Meter," *Review of Scientific Instruments*, **21**(3), pp. 219–225.

[4] Alexiev, D., M. I. Reinhard, L. Mo, and A. Rosenfeld (1999) "A transient conductance technique for characterisation of deep-level defects in highly irradiated detector-grade silicon," *Nuclear Instruments and Methods in Physics Research Section A: Accelerators, Spectrometers, Detectors and Associated Equipment*, **434**(1), pp. 103–113.

[5] Gauzzi, A., J. L. Cochec, G. Lamura, B. J. Jönsson, V. A. Gasparov, F. R. Ladan, B. Plaçais, P. A. Probst, D. Pavuna, and J. Bok (2000) "Very high resolution measurement of the penetration depth of superconductors by a novel single-coil inductance technique," *Review of Scientific Instruments*, **71**(5), pp. 2147–2153.

[6] McIver, R. T., Jr. (1973) "A Solid-State Marginal Oscillator for Pulsed Ion Cyclotron Resonance Spectroscopy," *Review of Scientific Instruments*, **44**(8), pp. 1071–1074.

[7] Warnick, A., L. R. Anders, and T. E. Sharp (1974) "A marginal oscillator detector for ion cyclotron resonance spectrometers," *Review of Scientific Instruments*, **45**(7), pp. 929–935.

[8] Miller, G. L., M. Soni, and R. L. Fenstermacher (1982) "A technique for investigating the properties of surfaces, thin films, and interfaces by means of a mechanical marginal oscillator," *Journal of Applied Physics*, **53**(2), pp. 979–983.

[9] Thomas III, L. J. (1988), "Marginal Oscillator for Acoustic Monitoring of Curing of Plastics," U.S. Patent 4 758 803.

[10] Robinson, F. N. H. (1988) "An accurate measuring instrument for capacitance above 0.01 microfarad," *Journal of Physics E: Scientific Instruments*, **21**(3), pp. 257–258.

[11] Betts, D. S., D. T. Edmonds, B. E. Keen, and P. W. Matthews (1964) "A susceptibility thermometer for use at very low temperatures," *Journal of Scientific Instruments*, **41**(8), pp. 515–516.

[12] Viswanathan, T. L., T. R. Viswanathan, and K. V. Sane (1975) "A Study of Marginal Oscillator Behavior," *IEEE Transactions on Instrumentation and Measurement*, **24**(1), pp. 55–61.

[13] Adler, M. S. and S. D. Senturia (1969) "Calibrated Sensitivity Measurements of Nuclear Magnetic Resonance Spectrometers," *Review of Scientific Instruments*, **40**(11), pp. 1481–1483.

[14] Miller, D., J. L. Schiano, and T. Tyson (2009) "Comparison of Predicted, Simulated, and Experimentally Measured Conversion Gain in a Robinson Marginal Oscillator," *NSF EE REU PENN STATE Annual Research Journal*, **VII**.

[15] Tricou, B. (2011), "Analysis, Design, and Synthesis of a Negative Resistance Converter for a Marginal Oscillator," The Pennsylvania State University.

[16] Stremler, F. G. (1982) *Introduction to Communication Systems*, 2nd ed., Addison-Wesley, Reading, Mass.

[17] Blaquiere, A. (1966) *Nonlinear system analysis*, Academic Press, New York.

[18] Rychak, R. S. (2009), "Method and Instrumentation for Determining the Sensitivity of a Robinson Marginal Oscillator," The Pennsylvania State University.

[19] Dahlquist, G. (1973) "Problems Related to the Numerical Treatment of Stiff Differential Equations," in *International Computing Symposium* (E. G. et al., ed.), North Holland, 1974, pp. 307–314.

[20] Liniger, W. (1972–1973) "Solution Numériques des Équations Différentielle et au derivées partielle," Unpublished Lecture Notes of a course taught at Swiss Federal Institute of Technology, Lausanne, Switzerland.

[21] Curtiss, C. F. and J. O. Hirschfelder (1952) "Integration of Stiff Equations," *Proc. Nat. Acad. Science U.S.*, **38**, pp. 235–243.

[22] Brugnano, L., F. Mazzia, and D. Trigiante (2011) "Fifty Years of Stiffness," in *Recent Advances in Computational and Applied Mathematics* (T. E. Simos, ed.), Springer Netherlands, pp. 1–21.

[23] Shampine, L. F., M. W. Reichelt, and K. J. A. (1999) "Solving Index-1 DAEs in MATLAB and Simulink," *SIAM Review*, **41**, pp. 538–552.

[24] Shampine, L. F. and M. E. Hosea (1996) "Analysis and Implementation of TR-BDF2," *Applied Numerical Mathematics*, **20**, pp. 21–37.

[25] Shampine, L. F. and M. W. Reichelt (1997) "The MATLAB ODE Suite," *SIAM J. on Scientific Computing*, **18**, pp. 1–22.

[26] Suits, B. H., A. N. Garroway, and J. B. Miller (1998) "Super-Q Detection of Transient Magnetic Resonance Signals," *Journal of Magnetic Resonance*, **132**, pp. 54–64.

Appendix A

Equivalent Bandwidth of a Parallel RLC Circuit

The equivalent bandwidth of a system is the bandwidth of an ideal brick-wall filter that gives the same noise power as the actual system. Assuming white noise and a system with a transfer function $H(j\omega)$, Stremler gives the equivalent bandwidth as [16]

$$B_{eq} = \frac{\int_0^\infty |H(j\omega)|^2 \, d\omega}{|H(j\omega_0)|^2}, \tag{A.1}$$

where ω_0 is the midband frequency that maximizes $|H(j\omega)|$. This definition is illustrated in Figure A.1.

This thesis wants to find the equivalent bandwidth of a parallel RLC circuit. From Eq. (2.9),

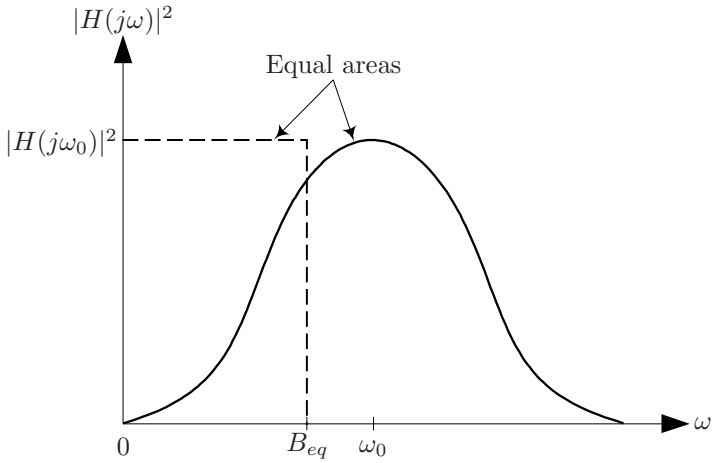

Figure A.1. Graphic definition of equivalent bandwidth.

the transfer function that relates the noise current $i_n(t)$ to the voltage $v(t)$ is

$$H(j\omega) = \frac{\frac{1}{C}j\omega}{(j\omega)^2 + \frac{\omega_n}{Q}j\omega + \omega_n^2}. \tag{A.2}$$

It follows that

$$|H(j\omega)|^2 = \frac{\omega^2/C^2}{(\omega^2 - \omega_n^2)^2 + \frac{\omega_n^2}{Q^2}\omega^2}. \tag{A.3}$$

Using $\omega_0 = \omega_n$ for a parallel RLC circuit, it follows from Eq. (A.3) that

$$|H(j\omega_0)|^2 = \frac{1}{C^2}\frac{Q^2}{\omega_n^2}. \tag{A.4}$$

Using the equivalent bandwidth definition in Eq. (A.1), it follows from Eqs. (A.3) and (A.4) that

$$B_{eq} = \frac{\omega_n^2}{Q^2}\int_0^\infty \frac{\omega^2}{\omega^4 + \left(\frac{\omega_n^2}{Q^2} - 2\omega_n^2\right)\omega^2 + \omega_n^4}\, d\omega. \tag{A.5}$$

Because the integrand in Eq. (A.5) is an even function of ω, the integral can be expressed equivalently as

$$B_{eq} = \frac{\omega_n^2}{2Q^2}\int_{-\infty}^\infty \frac{\omega^2}{\omega^4 + \left(\frac{\omega_n^2}{Q^2} - 2\omega_n^2\right)\omega^2 + \omega_n^4}\, d\omega. \tag{A.6}$$

The integral in Eq. (A.6) is difficult to evaluate using elementary calculus but is easily evaluated using contour integration. To see this, consider integrating the complex function

$$f(z) = \frac{\omega_n^2}{2Q^2}\frac{z^2}{z^4 + \left(\frac{\omega_n^2}{Q^2} - 2\omega_n^2\right)z^2 + \omega_n^4} \tag{A.7}$$

along the contour $\mathcal{A}$ shown in Figure A.2, which consists of the line segment along the real axis

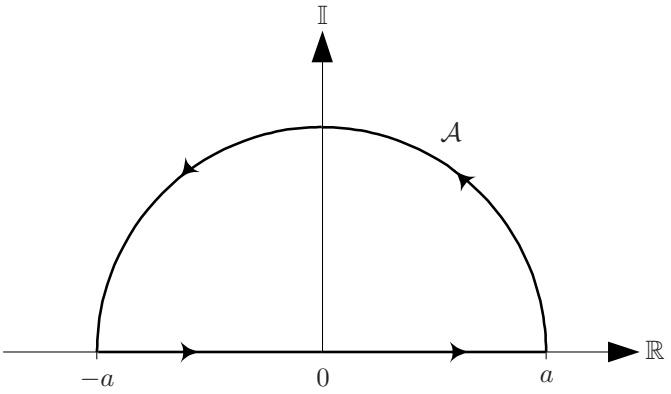

Figure A.2. Contour $\mathcal{A}$ of integration.

from $-a$ to a and the semicircle in the upper half-plane centered at the origin. Choose a large enough such that both poles of $f(z)$ in the upper hand-plane are contained in $\mathcal{A}$. This integral can be found by noting that $f(z)$ has two poles in the upper half-plane, and the sum of their residues is

$$\sum \text{Res} = \frac{\omega_n}{4Qj}. \tag{A.8}$$

It follows from the residue theorem that

$$\oint_{\mathcal{A}} f(z)\,dz = 2\pi j \sum \text{Res} = \frac{\pi\omega_n}{2Q} \tag{A.9}$$

for sufficiently large a. All that remains is to show that

$$B_{eq} = \oint_{\mathcal{A}} f(z)\,dz. \tag{A.10}$$

Note that

$$\oint_{\mathcal{A}} f(z)\,dz = \int_{-a}^{a} f(z)\,dz + \int_{\text{Arc}} f(z)\,dz. \tag{A.11}$$

Using the estimation lemma, it can be shown that

$$\left|\int_{\text{Arc}} f(z)\,dz\right| \leq \frac{\omega_n^2}{2Q^2}\frac{\pi a^3}{a^4 + \left|\frac{\omega_n^2}{Q^2} - 2\omega_n^2\right| a^2 + \omega_n^4} \to 0 \text{ as } a \to \infty, \tag{A.12}$$

which means

$$\int_{\text{Arc}} f(z)\,dz \to 0 \text{ as } a \to \infty \tag{A.13}$$

by the sandwich theorem. Using Eqs. (A.11) and (A.13), it follows that

$$\oint_{\mathcal{A}} f(z)\,dz = \int_{-a}^{a} f(z)\,dz \text{ as } a \to \infty. \tag{A.14}$$

Using Eqs. (A.9) and (A.14), this thesis finds the equivalent bandwidth to be

$$B_{eq} = \int_{-\infty}^{\infty} f(z)\,dz = \lim_{a\to\infty}\int_{-a}^{a} f(z)\,dz = \oint_{\mathcal{A}} f(z)\,dz \tag{A.15}$$

$$= \frac{\pi\omega_n}{2Q} \text{ rad/s}. \tag{A.16}$$

Using Eq. (2.8), it can be equivalently expressed as

$$B_{eq} = \frac{\pi}{2RC} \text{ rad/s}. \tag{A.17}$$

Note that the equivalent bandwidth is inversely proportional to the Q-factor. Therefore, the thermal noise seen across the resonant circuit decreases as the Q-factor increases. Also, the

equivalent bandwidth is related to the 3 dB bandwidth β by

$$B_{eq} = \frac{\pi}{2}\beta. \tag{A.18}$$

Interestingly, this is the same relationship found between the equivalent and 3 dB bandwidths of a first-order Butterworth filter.

Appendix B

Academic Vita

Name: Klaus K. Zhang

Address: 926 Dylan Drive
Allentown, PA 18104

Email: kkz5003@psu.edu

Education:
The Pennsylvania State University, University Park, PA
B. S. in Electrical Engineering, May 2011

Honors: Schreyer Honors College

Thesis Title: *Conversion Gain and Sensitivity in Marginal Oscillators: Continuous and Sampled-Data Negative Resistance Converters*

Thesis Supervisor: Jeffrey L. Schiano
Associate Professor of Electrical Engineering